Schmidt, Fabian ; Swiderek, Petra ; Bredehöft, Jan Hendrik

Electron-Induced Processing of Methanol Ice

Journal Article as: peer-reviewed accepted version (Postprint)

DOI of this document*(secondary publication): https://doi.org/10.26092/elib/3709

Publication date of this document: 19/02/2025

* for better findability or for reliable citation

Recommended Citation (primary publication/Version of Record) incl. DOI:

Electron-Induced Processing of Methanol Ice
Fabian Schmidt, Petra Swiderek, and Jan H. Bredehöft
ACS Earth and Space Chemistry 2021 5 (2), 391-408
DOI: 10.1021/acsearthspacechem.0c00250

Electron-Induced Processing of Methanol Ice

*Fabian Schmidt, Petra Swiderek, and Jan H. Bredehöft**

Universität Bremen, Institut für Angewandte und Physikalische Chemie,

Fachbereich 2 (Chemie/Biologie), Leobener Straße / NW 2,

Postfach 330440, D-28334 Bremen, Germany

*Correspondence:

Corresponding Author

jhbredehoeft@uni-bremen.de

Keywords: Astrochemistry, Mechanisms, UHV, Physical Chemistry, Methanol, Low Energy Electrons

Abstract

The formation of methane (CH_4), formaldehyde (H_2CO), ethylene glycol ($HOCH_2CH_2OH$), methoxymethanol (CH_3OCH_2OH), dimethyl ether (CH_3OCH_3), and ethanol (CH_3CH_2OH) upon electron irradiation of condensed multilayer adsorbates of CH_3OH as model of cosmic CH_3OH ice has been monitored by the combined use of electron-stimulated and thermal desorption experiments. The energy-dependent relative yields of all products were measured between 2.5 eV and 20 eV and reaction mechanisms of product formation deduced. The energy dependences of the yields of $HOCH_2CH_2OH$, CH_3OCH_2OH,

CH_3OCH_3, and CH_3CH_2OH agree closely with their threshold at the lowest electronic excitation energy of CH_3OH. Formation of these products is consequently ascribed to reactions of radicals formed by dissociation of neutral electronically excited states and, at higher energy, also by ionization and subsequent proton transfer to an adjacent CH_3OH. These electron-molecule interactions also can contribute to the non-resonant formation of H_2CO and CH_4, these latter products are also produced through resonances around 4 eV reported previously from anion ESD experiments and around 13 eV seen earlier in the energy-dependent yield of CO. The present results constitute the most complete data set on the energy dependence of product formation during low-energy electron exposure of condensed CH_3OH so far. They provide a comprehensive picture of the reactions triggered by electron impact with energies in the range between 2.5 eV and 20 eV as representative of low-energy secondary electrons that are released from condensed material, for instance, under the effect of cosmic radiation.

Introduction

Following carbon monoxide (CO) and water (H_2O), methanol (CH_3OH) is among the most common molecules found in interstellar ices.[1] There are numerous studies on chemical reactions in pure CH_3OH ices induced by energetic processing. Specifically, energetic processing has been investigated by low-energy electrons (≤ 20 eV),[2–6] higher energy electrons (5 keV),[6–14] X-Ray radiation,[15] UV radiation,[16–19] and ion irradiation.[20–24] The span of products that were identified encompasses, among others, methane (CH_4),

formaldehyde (H_2CO), ethylene glycol ($HOCH_2CH_2OH$), methoxymethanol (CH_3OCH_2OH), dimethyl ether (CH_3OCH_3), and ethanol (CH_3CH_2OH) which are depicted in Chart 1. These molecules are typically considered to be produced either by unimolecular decomposition of CH_3OH or by radical recombination among the first generation of dissociation products.[7,11,16] Further electron exposure leads to depletion of these initially formed products yielding CO, carbon dioxide (CO_2), acetaldehyde ($HC(O)CH_3$), methyl formate ($HC(O)OCH_3$), glycolaldehyde ($HC(O)CH_2OH$) (see also Chart 1), and a number of minor products (not shown in Chart 1).[2,11] Considering the high number of irradiation products, CH_3OH is discussed as an important feedstock for the production of organic compounds in space.[13]

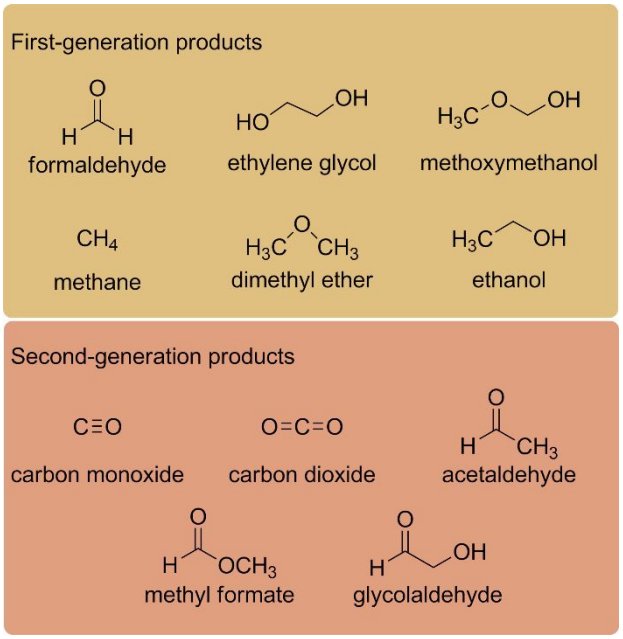

Chart 1. Structural formulae of some typically observed first- and second-generation products. First-generation products are thought to be produced directly by decay of CH_3OH or by radical recombination among the first generation of dissociation products. In contrast, the second generation of products is thought to be produced by further

depletion of the initially formed products. All of these compounds have been reported to form upon electron irradiation of CH_3OH ice.[2–11] Note that other products might also be regarded as first- and second-generation products but are not included in this chart.

In a typical experiment, multilayer ices of CH_3OH are exposed to a radiation source and changes in composition are monitored by suitable analytical tools. In many of the above studies, infrared (IR) spectroscopy has been used as the only tool to identify stable products and intermediates as well as to monitor reaction progress.[9,17,20–24] This has enabled the identification of the formyl ($HCO^{\bullet}$) and hydroxymethyl ($^{\bullet}CH_2OH$) radicals as intermediates.[16] The downside of IR spectroscopy is that definite band assignment as well as quantification is difficult to impossible for organics with similar functional groups because the corresponding bands often lie within a narrow range of wavenumbers and bands tend to become broad in the condensed phase due to interactions of nearby molecules. Further complicating is the fact that for some less stable compounds and intermediates reference IR spectra do not exist. Some of the more recent studies thus tried to circumvent these limitations in part by using mass spectrometry in combination with desorption techniques. This approach allowed Harris et al. to identify the previously unknown radiolysis product CH_3OCH_2OH and to observe the desorption of $CH_3^{\bullet}$ upon irradiation.[13] Much effort has been made to identify less abundant products and to improve quantification by using more sophisticated techniques including thermal desorption spectrometry (TDS) combined with single photon ionization reflectron time of flight mass spectrometry (SPI ReTOF-MS),[11,25] gas chromatography coupled to mass spectrometry (GC-MS),[12,19] and laser ablation coupled to time of flight mass spectrometry.[26] However,

while the formation of the molecules depicted in Chart 1 is commonly accepted, the mechanisms that drive their formation just start to emerge.[3,7,10–12,14,16] There are already a number of publications covering the temporal evolution of product yields and that of some intermediates during irradiation[7–9,15,16,26] as well as upon annealing of the ice.[16,26] However, little is still known about the initial dissociation events that underly product formation. This is because typical experiments with broadband UV lamps or higher energy radiation like keV electrons do not allow to distinguish between different dissociation channels of CH_3OH, although some attempts have been made to extract information from the temporal evolution of product yields[7] and from isotopic labeling.[11,12,14]

Boyer et al.[3] and Lepage et al.[4] addressed this issue by investigating the dependence of product yields on electron energy. This enabled them to identify the primary electron-molecule interactions which is essential to obtain a comprehensive picture of the underlying reactions responsible for product formation. In particular, they used low-energy electrons with E_0 = 0–20 eV. This energy range is typical of secondary electrons released in vast numbers when ionizing radiation interacts with solid ices.[27] The results of these experiments are thus also of relevance for experiments with other kinds of radiation sources. In addition, experiments with low-energy electrons enable one to promote or supress the formation of specific reactive species by tuning the electron energy. By this, the number of products can be reduced, which, in turn, facilitates their identification. More specifically, electrons can induce the formation of reactive species by either of three mechanisms: Formation of radical cations by electron-impact ionization (EI), of transient

negative ions (TNI) by electron attachment (EA) or of electronically excited molecules by electron excitation (EE).[27,28]

Above but near the ionization threshold, EI typically produces intact molecular cations. At electron energies that exceed the ionization threshold by at least the energy required to dissociate a chemical bond, dissociative ionization (DI) can produce radical and cationic fragments of the molecular ion.[28] Molecular rearrangement combined with the formation of new bonds, however, can lower this additional energy.[29] The yield of ions produced by EI and DI typically increases with electron energy once the ionization threshold or a characteristic appearance energy is reached.[27] In contrast, EA processes often occur below the ionization threshold and are particularly dominant at near-thermal electron energies. EA only occurs in well-defined, narrow energy ranges called resonances and is often, but not necessarily, followed by dissociation of the TNI into an anion and one or more neutral species. This process is called dissociative electron attachment (DEA).[28] Following EE, a molecule can dissociate into neutral radicals which is called neutral dissociation (ND). Similar to EI and DI, ND shows a threshold-type increase of fragment yields with increasing electron energy.[27] The role of ND, however, often remains unclear because it is difficult to monitor this electron-molecule interaction experimentally, as no charged species are formed.[30]

Reactive species produced by these electron-molecule interactions can react with other molecules and thus lead to formation of stable products. The initial electron-molecule

interactions can then be distinguished by investigating the dependence of product yield on electron energy. Although Lepage et al.[4] and Boyer et al.[3] performed such experiments, only the energy dependences of CO, $HOCH_2CH_2OH$ and CH_3OCH_2OH have been investigated so far. Therefore, we investigate here the formation of CH_4, H_2CO, CH_3OCH_3, and CH_3CH_2OH and its dependence on the electron energy and revisit also the formation of $HOCH_2CH_2OH$ and CH_3OCH_2OH already reported by Boyer et al.[3] In particular, we focus on low-energy electrons (≤20 eV) which encompasses the characteristic regimes of all fundamental electron-molecule interactions, namely EA and DEA, ND, as well as EI and DI. These initiating processes are distinguished by observing the energy dependence of product formation.

Experimental Section

The electron-induced chemistry in cryogenic films of CH_3OH (VWR, Normapur) was studied by electron-stimulated desorption (ESD) and post-irradiation TDS. Experiments were performed in an ultrahigh-vacuum (UHV) chamber evacuated by turbomolecular pumps. The base pressure inside the UHV chamber was below the detection limit of the ion gauge (AML) which is about 3×10^{-11} mbar as stated by the manufacturer. CH_3OH was degassed by several freeze–pump–thaw cycles before leaking it into the chamber. Condensed films of CH_3OH were prepared by introducing defined amounts of gas into the vacuum chamber from a gas handling manifold allowing them to condense on a polycrystalline Ta substrate held at a temperature of ~35 K by a closed-cycle helium

cryostat. The amounts of CH_3OH introduced into the chamber were controlled by monitoring the pressure drop in the gas handling manifold with an MKS Baratron type 622B capacitance manometer. Monolayer calibration for CH_3OH was performed using a set of TDS experiments for various initial surface coverages as controlled by the pressure drop.

In the range of low amounts of deposited material, a broad monolayer desorption peak of CH_3OH is seen with maximum shifting from 143 K to 137 K. With further deposition of CH_3OH, a second peak at 132 K assigned to formation of a bilayer appears and saturates for pressure drops in the gas handling manifold around 5 mTorr. At this pressure drop, a signal assigned to multilayer desorption emerges at 129 K (Figure S1**Error! Reference source not found.**). Eventually, multilayer desorption dominates over bi- and monolayer desorption and the leading edges of the multilayer desorption signals coincide (Figure S2) which is characteristic of multilayer desorption. For thicker films, a fourth desorption peak at 132 K emerges which can be assigned to a phase transition from amorphous to crystalline CH_3OH ice which occurs just before desorption. This phase transition was observed for multilayer ices of CH_3OH beforehand by Bolina and et al.[31] and is a well-known effect in the case of amorphous solid water.[32,33] Note that this phase transition requires heating of the film[31] and that the as-deposited CH_3OH in this study is in an amorphous rather than crystalline state. Because there is no distinct monolayer peak, accurate calibration of film thickness would require fitting of the monolayer, bilayer and multilayer peaks to the overall signal. The concomitant phase transition, however, makes

this task difficult. Comparing the amounts of CH_3OH with film thicknesses obtained by depositing H_2O and C_2H_4 under similar conditions,[34,35] however, suggest an approximate film thickness of 12 ± 4 monolayers for a pressure drop of 30 mTorr in the gas handling manifold. Taking the density of crystalline CH_3OH ice into account (1.01 ± 0.03 g/cm³),[36] 12 monolayers should correspond to a thickness of about 4.5 nm (see Supporting Information for calculation). This film thickness was used for all samples throughout the present study. Note that the uncertainty of the absolute film thickness is not to be confused with the reproducibility of the film thickness. Analysis of the as-deposited CH_3OH films by TDS revealed that film thickness varies by only about 2 % throughout the experiments based on the standard deviation of the integrated desorption signals.

Electron exposures were carried out with a commercial STAIB NEK-150-1 electron source with an energy resolution of 0.5 eV. The instrument allows for beam shaping which ensures that the whole sample is evenly irradiated at all energies. Neutral species that desorbed during irradiation were monitored using a quadrupole mass spectrometer (QMS) residual gas analyser (Stanford Research System RGA 200). The QMS has an ion source operating with electrons of energy E_0 = 70 eV. During TDS, the sample is annealed from 35 K to 450 K by resistive heating with a constant heating rate of 1 K/s. In a typical TDS, no more than four mass-to-charge ratios were monitored simultaneously in order to maintain a sufficiently high signal-to-noise ratio. Subsequently, the sample temperature was held at 450 K for another 2 min in order to desorb any remaining adsorbates. Analysis of the data was performed with Python[37] using the NumPy[38] and SciPy[39] packages. The

uncertainties of the integral intensities were determined by repeating some of the experiments and calculating the standard deviation where three or more repititions were made. Because the experiments are relatively time consuming, three or more repititions were only performed for a few representative data points.

Products were identified based on characteristic fragments in their mass spectra.[40] The identities of $HOCH_2CH_2OH$ and CH_3CH_2OH were further verified by comparing the desorption temperatures of the signals in the irradiated sample with those of the actual compounds. Because desorption temperatures can be very sensitive to the molecular environment,[41] we typically admix the pure substances to CH_3OH and perform TDS of the resulting film.[34,35] CH_3CH_2OH and $HOCH_2CH_2OH$, however, desorb at higher temperatures than CH_3OH. The molecular environment is thus not well represented by a pure CH_3OH matrix because other irradiation products might also influence the desorption temperature. Therefore, we deviated from this standard procedure and condensed distinct amounts of $HOCH_2CH_2OH$ (Sigma Aldrich, 99.8%) and CH_3CH_2OH (Merck, ≥99.8%) on top of a CH_3OH film after irradiation with 1000 μC/cm² at an electron energy of 20 eV. This electron dose equates to roughly one electron per molecule in the film.

The relative molecular abundance of a specific product was determined by comparing the areas under its ESD and TDS signals with that of CH_3OH in a non-irradiated sample. This comparison is based on the different cross sections for formation of the observed fragments inside the ionizer of the mass spectrometer, which are also known as partial

ionization cross sections. Fragments monitored during ESD and TDS have been chosen on the basis of characteristic mass-to-charge ratios as deduced from the mass spectra of the products (Figure S3). The fragment *m/z* = 16 was selected for CH_4, *m/z* = 30 for H_2CO, *m/z* = 31 for CH_3OH, *m/z* = 33 for $HOCH_2CH_2OH$, *m/z* = 61 for CH_3OCH_2OH, *m/z* = 46 for CH_3OCH_3, and *m/z* = 46 for CH_3CH_2OH. Note that the *m/z* = 31 signal of CH_3OH was only used for quantification of the non-irradiated film and thus does not interfere with the *m/z* = 31 fragments of other products. For a number of compounds, experimental values for ionization cross sections have not been reported. Therefore, total ionization cross sections were calculated by the Binary Encounter-Bethe (BEB) model.[42,43] The necessary orbital properties were obtained by calculation with the GAMESS software package,[44,45] while the ionization energies of the target molecules were taken from the NIST Chemical Webbook.[46] This resulted in 4.35 ± 0.05 Å² for CH_4, 3.98 ± 0.05 Å² for H_2CO, 5.26 ± 0.05 Å² for CH_3OH, 10.11 ± 0.05 Å² for $HOCH_2CH_2OH$, 9.6 ± 0.3 Å² for CH_3OCH_2OH, 8.14 ± 0.05 Å² for CH_3OCH_3, and 8.30 ± 0.05 Å² for CH_3CH_2OH. Uncertainties are largely determined by the errors of experimental ionization energies. The BEB cross section for CH_3OCH_2OH has a considerably larger uncertainty than for the other compounds because the experimental ionization energy has not been reported which would be required to obtain a more accurate result. This latter cross section was thus estimated from similar-sized compounds. Partial ionization cross sections were then obtained by multiplying the absolute ionization cross section with the relative intensity of the respective ion, as deduced from the mass spectrum, divided by the sum of intensities

over all ions. In order to account for possible differences in detection efficiencies and quadrupole transmission factors, mass spectra of pure CH_4 (Messer, ≥99.995%), H_2CO (obtained by heating paraformaldehyde; Riedel-de Haën, ≥95.0%), CH_3OH, $HOCH_2CH_2OH$, and CH_3CH_2OH have been recorded with the same mass spectrometer used for TDS experiments, showing no significant deviations from published mass spectra.[40] In the case of CH_3OCH_3[40] and CH_3OCH_2OH [47], we deduced the relative ion intensities from published mass spectra because CH_3OCH_3 and CH_3OCH_2OH have not been commercially available, and CH_3OCH_2OH is a labile compound which makes it difficult to handle.[47] For the relative intensities of CH_4, H_2CO, CH_3OH, $HOCH_2CH_2OH$, and CH_3CH_2OH we estimate an uncertainty of 15 % due to pressure fluctuations upon recording the mass spectra. Within these error margins, the intensity ratios for different fragment signals in the TDS agree with those from the mass spectra. For CH_3OCH_3, we assume the uncertainty to be the same. We note, however, that the intensities of higher mass-to-charge ratios are typically slightly lower than in the NIST spectra. We thus tend to underestimate the abundance of dimethyl ether. In the case of CH_3OCH_2OH, it is more difficult to estimate the uncertainty of the intensities because contributions of thermal decomposition of CH_3OCH_2OH into CH_3OH and H_2CO could not be ruled out in the mass spectrum reported previously.[47] Comparison of the TDS intensitites of the m/z = 61 and m/z = 33 fragments of CH_3OCH_2OH, however, suggests that the intensities in the mass spectrum of CH_3OCH_2OH have uncertainties of no more than 30 %.

The uncertainties of the partial ionization cross sections were calculated from the individual uncertainties of the relative intensities in the mass spectrum and that of the ionization cross section by using standard error propagation. Following this procedure, the partial ionization cross sections at 70 eV were calculated to be 2.0 ± 0.3 Å² for the *m/z* = 16 parent ion of CH_4, 1.3 ± 0.2 Å² for the *m/z* = 30 parent ion of H_2CO, 1.57 ± 0.25 Å² for the *m/z* = 31 fragment of CH_3OH, 1.3 ± 0.2 Å² for the *m/z* = 33 fragment of $HOCH_2CH_2OH$, 1.9 ± 0.6 Å² for the *m/z* = 61 fragment of CH_3OCH_2OH, 2.1 ± 0.3 Å² for the *m/z* = 46 parent ion of CH_3OCH_3, and 0.47 ± 0.07 Å² for the *m/z* = 46 parent ion of CH_3CH_2OH. Uncertainties of the relative molecular abundances were then calculated from the uncertainties of the partial ionization cross sections and those of the integral intensities using standard error propagation.

The Gibbs free Energy of the formation of H_2CO from CH_3OH by elimination of H_2 was calculated using a method modified from the G3MP2B3 calculations presented by Janoschek and Rossi.[48] Differing from their method, the geometry was optimized using the B3LYP functional with an augmented correlation-consistent polarized Valence-only Triple-Zeta (aug-cc-pVTZ) basis set.[49] The energy of the system was evaluated using size-consistent quadratic interactions with unlinked triples (QCISD(T))[50] with the same basis set. The extrapolation to the basis set limit was achieved by two MP2[51] calculations, the first with the same basis set, and the second using aug-cc-pV Quadruple-Zeta.[49] The final energy was calculated as the QCISD(T) energy corrected for the difference between the MP2 calculations, the zero-point energy and a term for higher level correlation as described in full detail by Janoschek and Rossi[48]. The Gibbs Free Energy was calculated as G = H - TS, with the enthalpy H = energy + kT and the entropy S derived from frequency analysis of the B3LYP geometry optimization at 35 K. All calculations were performed using the ORCA 4.2.1[52,53]quantum chemistry program package.

Results and Discussion

Identification of Products

To identify products formed by electron-induced reactions, we irradiated multilayer films of CH_3OH with electrons of E_0 = 20 eV and electron exposures of 1000 µC/cm². During irradiation, mass spectra were recorded in the range from *m/z* = 10 to *m/z* = 50 which allows identification of desorbing species. A sudden increase of the mass spectrometric signals of several mass-to-charge ratios is observed with beginning electron irradiation due to ESD (Figure 1). The ESD signals at *m/z* = 31 and 32 revealed the desorption of CH_3OH. Some of the observed signals at lower mass-to-charge ratios (*m/z* = 15, 16, 28, 30), however, are significantly more intense than is expected from the mass spectrum of CH_3OH (Figure S3) which suggests the formation of new products. This is further corroborated by careful inspection of the ESD signals which reveals that the increase of the *m/z* = 16 and 28 signals is delayed compared to the ESD signals of CH_3OH and must thus stem from an irradiation product.

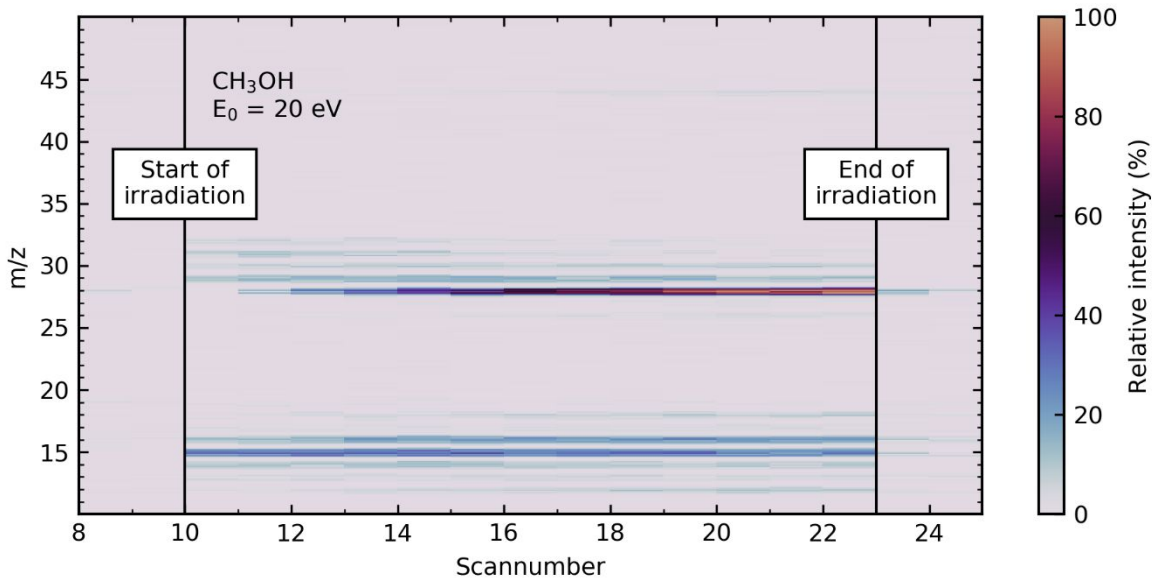

Figure 1. Evolution of ESD mass spectrometric signals with increasing number of scans during a 1000 µC/cm² electron irradiation of a multilayer CH_3OH film at E_0 = 20 eV. The two vertical lines mark the beginning (scannumber 10) and end of irradiation (scannumber 23) as was controlled by a negative bias on the sample. The colour code indicates the baseline corrected mass spectrometric signal increasing from low intensity (grey) over mid intensity (blue) to high intensity (red/yellow). The first and last seven scans are not displayed in order to focus on the actual irradiation.

The intensity ratios obtained from the mass spectra in Figure 1 might not reflect the true ratio of desorbing compounds because it takes about 20 s to record a single mass spectrum and because ESD signal intensities evolve with time. Thus, we repeated the irradiation but monitored only those mass-to-charge ratios (*m/z* = 14, 15, 16, 28, 29, 30, 31, and 32) that showed a significant signal in the ESD in order to achieve a reasonable time resolution. The so obtained ESD signals (see Figure S4**Error! Reference source not found.**) can be integrated over time which yields an averaged ESD mass spectrum (Figure 2, hollow bars). We think that this averaged mass spectrum reflects the signal

ratios more accurately than the single mass spectra from Figure 1. The uncertainty of the so-obtained mass spectrum is mainly determined by the signal-to-noise ratio of the ESD signals. We estimate this uncertainty to be 10 % with respect to the integrated ESD signal.

For deconvolution of the so-obtained spectrum, we used a protocol that was already used in the Cometary Sampling and Composition (COSAC) experiment.[54] We reduced the short list of candidate molecules to CH_3OH, H_2CO, CO, and CH_4 because these products were already reported in literature and we did not observe any signals higher than *m/z* = 32 in ESD. The fit was performed in order of decreasing mass, starting from *m/z* = 32. With this protocol, a good fit to the integrated ESD signals was obtained with exception of the *m/z* = 14 and 15 signals (Figure 2). We propose, that intact $CH_3^{\bullet}$ radicals desorb from the sample and thus contribute to these signals. The results of Harris et al.,[13] and Warneke and Swiderek,[55] who already observed desorption of intact $CH_3^{\bullet}$ radicals during electron irradiation of CH_3OH and acetone, respectively, can be regarded as proofs of principle that underline our interpretation.

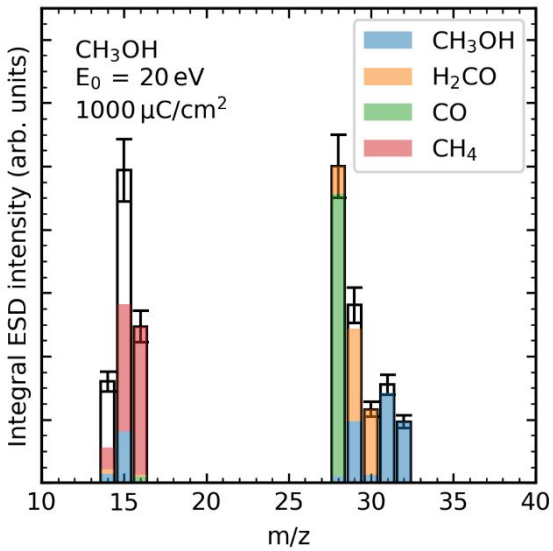

Figure 2. Comparison of the mass spectrum obtained from the data recorded during ESD at 20 eV (hollow bars) and the spectrum reconstructed by fitting the mass spectra of CH_4 (red bars), H_2CO (orange bars), CH_3OH (blue bars), and CO (green bars) to the ESD mass spectrum. The ESD mass spectrum was obtained by the areas under the desorption signals of *m/z* = 14, 15, 16, 28, 29, 30, 31, and 32 monitored during electron irradiation of multilayer films of CH_3OH with 1000 μC/cm² at E_0 = 20 eV. The mass spectra of CH_3OH, H_2CO, CO, and CH_4 were recorded with the same mass spectrometer used for recording the ESD mass spectrum. Error bars denote the uncertainty of the intergated ESD signals which has been estimated to be 10 %.

Post-irradiation TDS was performed to monitor substances that were retained in the irradiated film. After an electron exposure of 1000 μC/cm² at 20 eV, depletion of CH_3OH can be observed in the TDS along with the formation of a series of products. In line with the ESD data, the formation of CO (Figure S5**Error! Reference source not found.**), H_2CO (Figure 3), and CH_4 (Figure 4) indicates electron-induced degradation of CH_3OH upon irradiation. In addition, TDS revealed the formation of more complex molecules not seen in ESD, namely, $HOCH_2CH_2OH$ and CH_3OCH_2OH (Figure 5 and Figure 6), as well as

CH_3OCH_3 and CH_3CH_2OH (Figure 7 and Figure 8). The identification of these products is supported by the arguments summarized in the following paragraph. Further signals can be assigned to methyl formate, and possibly glycolaldehyde (Figure S6). All of these complex molecules are indicative of electron-induced synthesis because multiple molecules and/or reactive species must be involved in their formation. In the present study, we focus on the formation of H_2CO, CH_4, $HOCH_2CH_2OH$, CH_3OCH_2OH, CH_3OCH_3, and CH_3CH_2OH because these molecules are considered to be produced either by unimolecular decomposition of CH_3OH or by reactions of the first generation of dissociation products.

H_2CO was identified by its characteristic mass-to-charge ratios m/z = 29, and 30 (Figure S3). It shows a desorption signal at 88 K (Figure 3) which is in line with earlier experiments.[34]

CH_4 was identified by its characteristic mass-to-charge ratios m/z = 15 and 16 (Figure S3) and shows two desorption features at 50 K and 104 K (Figure 4). The first of these signals coincides closely with the multilayer desorption temperature of CH_4 and is thus characteristic of physisorbed CH_4.[41] The second desorption signal overlaps in part with that of H_2CO. The mass spectrum of H_2CO, however, does not show any fragment with m/z = 15 and only a very weak signal at m/z = 16 (about 2.4% of the m/z = 30 signal intensity, Figure S3**Error! Reference source not found.**). The integral intensity of the m/z = 16 signal at 104 K in the irradiated sample, in contrast, is about three times higher

than that of the *m/z* = 30 signal and can thus not stem from fragmentation of H_2CO (Figure 4). We thus assign this second signal to trapping of CH_4 in the CH_3OH matrix which either co-desorbs with H_2CO or gets released when the CH_3OH molecules become more mobile. This is in line with other studies where significant trapping of CH_4 in CH_3OH ice was reported.[6,16,26]

$HOCH_2CH_2OH$ was identified by its characteristic mass-to-charge ratios at *m/z* = 31, 33, and 62 (Figure S3) and desorbs between 186 K and 220 K depending on its amount (Figure 5). The observed desorption temperature agrees well with those reported by Boyer et al.[3] and Harris et al.[13] which is 205 K and that of Boamah et al.[2] which is 215 K. Its identity was further verified by condensing different amounts of pure $HOCH_2CH_2OH$ on top of a CH_3OH film preirradiated at 20 eV with 1000 μC/cm² and performing TDS on the resulting film (Figure 6, left panel). In addition to the desorption signal present after irradiation, the signal intensity increases linearly with the amount of $HOCH_2CH_2OH$ condensed on top of the irradiated sample which corroborates our assignment (Figure 6, right panel).

CH_3OCH_2OH was identified by its characteristic mass-to-charge ratios *m/z* = 33 and 61 (Figure S3**Error! Reference source not found.**) and desorbs between 156 K and 175 K (Figure 5) depending on its amount. The observed desorption temperature is also in good agreement with that found by Schneider et al.,[18] Boyer et al.,[3] and Boamah et al.[2] who reported values between 155 K and 170 K.

CH_3OCH_3 and CH_3CH_2OH were both identified by their characteristic mass-to-charge ratios at *m/z* = 45 and 46 (Figure S3**Error! Reference source not found.**). The desorption signal of CH_3OCH_3 peaks between 95 K and 110 K (Figure 7) and agrees well with the desorption temperatures found by Boamah et al.[2] and Harris et al.[13] who reported values between 95 K and 115 K. The desorption signal of CH_3CH_2OH peaks between 148 K and 162 K, which is in line with the desorption temperature of 165 K found by Boamah et al.[2]. Note that the *m/z* = 45 fragments of CH_3OCH_2OH (Figure S3) and $HOCH_2CH_2OH$ overlap in part with that of CH_3CH_2OH as can be seen from the position of the *m/z* = 61 fragment of CH_3OCH_2OH and *m/z* = 62 fragment of $HOCH_2CH_2OH$ in Figure 7. We thus used the *m/z* = 46 fragment for quantification of CH_3CH_2OH. The identity of CH_3CH_2OH was further verified by condensing different amounts of CH_3CH_2OH on top of a CH_3OH film preirradiated at 20 eV with 1000 μC/cm² and performing TDS of the resulting film. In addition to the desorption signal at 152 K present after irradiation, the signal intensity increases linearly with the amount of CH_3CH_2OH condensed on top of the preirradiated film which corroborates our assignment (Figure 8).

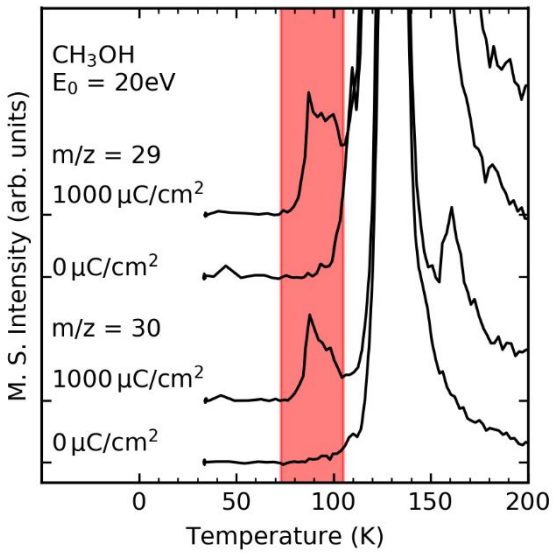

Figure 3. Thermal desorption spectra of a multilayer film of CH_3OH without electron exposure (denoted 0 µC/cm²) and after electron irradiation with 1000 µC/cm² at E_0 = 20 eV. The peaks at 88 K in the *m/z* = 29 and 30 curves (red) are assigned to H_2CO. The signals at 130 K in the *m/z* = 29 and 30 curves are assigned to fragments of CH_3OH, and the signal at 156 K in the *m/z* = 30 curve of the irradiated sample has been assigned to a fragment of CH_3OCH_2OH. Tick marks on the left and right axis indicate the vertical offset of the individual curves. The magnification is the same for all curves.

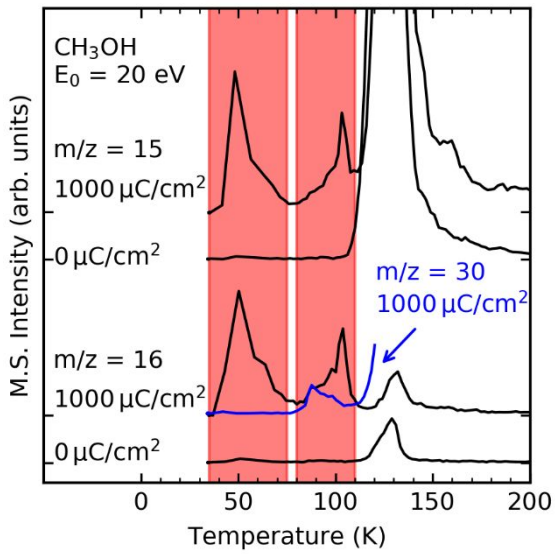

Figure 4. Thermal desorption spectra of a multilayer film of CH_3OH without electron exposure (denoted 0 µC/cm²) and after electron irradiation with 1000 µC/cm² at E_0 = 20 eV. The peaks at 50 and 104 K in the *m/z* = 15 and 16 curves (red) are assigned to CH_4. The signals at 130 K in the *m/z* = 15 and 16 curves are assigned to fragments of CH_3OH. The peak area of the *m/z* = 16 signal at 104 K is about three times higher than that of the *m/z* = 30 signal at 90 K (blue line, see also Figure 3). Comparing the ratio of these peak areas with the relative intensities of the *m/z* = 16 and 30 fragments in the mass spectrum of H_2CO (Figure S3) suggest that the signal at 104 K in the *m/z* = 16 curve does not stem from H_2CO but solely from CH_4. Tick marks on the left and right axis indicate the vertical offset of the individual curves. The magnification is the same for all curves.

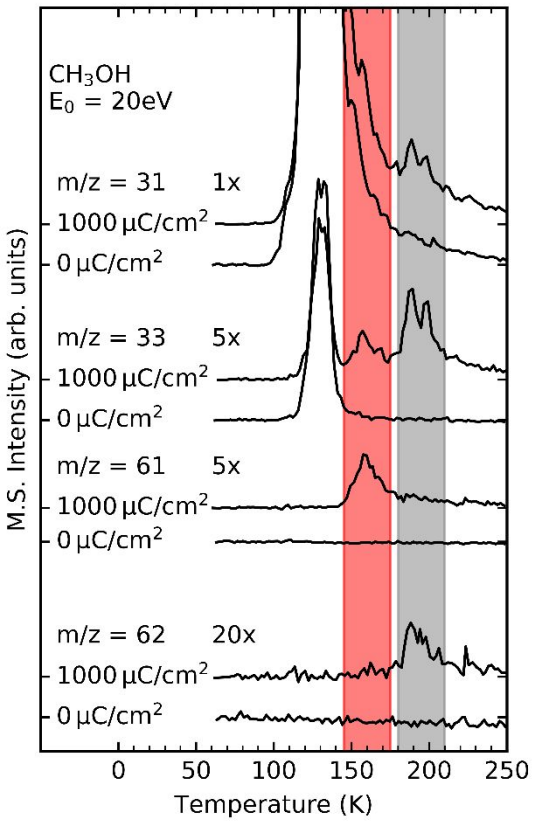

Figure 5. Thermal desorption spectra of a multilayer film of CH_3OH without electron exposure (denoted 0 μC/cm²) and after electron irradiation with 1000 μC/cm² at E_0 = 20 eV. The peaks at 130 K in the *m/z* = 31 and 33 curves of the irradiated and pristine sample are assigned to the CH_3O^+ fragment and the $^{13}CH_3OH^{\bullet+}$ isotopologue of CH_3OH, respectively. The peak at 156 K in the *m/z* = 33 and 61 curves (red) is assigned to CH_3OCH_2OH, and the peak at 192 K in the *m/z* = 31, 33, and 62 curves (grey) to $HOCH_2CH_2OH$ (see also the mass spectra in Figure S3). Noticeably, these peaks are only present in the irradiated sample which is indicative of electron-induced synthesis. Tick marks on the left and right axis indicate the vertical offset of the individual curves. The individual curves are magnified by the denoted factors.

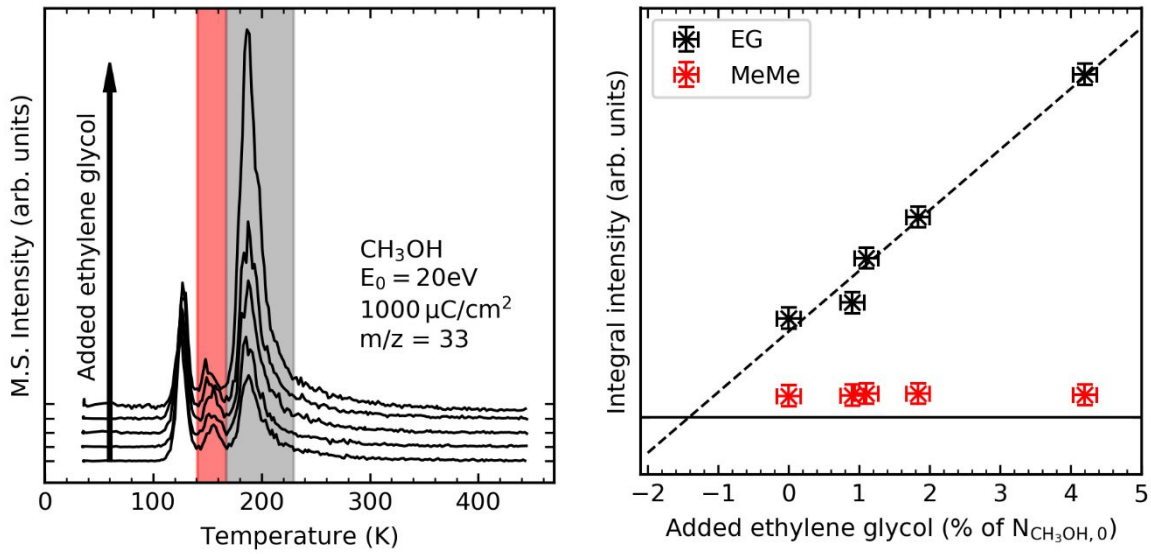

Figure 6. Thermal desorption spectra of a multilayer film of CH_3OH after electron irradiation with 1000 µC/cm² at E_0 = 20 eV (bottom spectrum in left panel). The peak at 130 K was assigned to the $^{13}CH_3OH^{\bullet+}$ isotopologue of CH_3OH, the peak at 156 K to CH_3OCH_2OH (MeMe, red), and the peak at 192 K to $HOCH_2CH_2OH$ (EG, grey). The assignment of the peak at 192 K in the *m/z* = 33 curve to $HOCH_2CH_2OH$ was further verified by admixing increasing amounts of $HOCH_2CH_2OH$ to the irradiated sample (left panel). This leads to a linear increase of peak area for the second signal at 192 K while the peak area of the first signal at 156 K remains constant (right panel). Tick marks on the left and right axis of the left panel indicate the vertical offset of the individual curves. The magnification is the same for all curves. The horizontal line in the right panel indicates an integral intensity of zero.

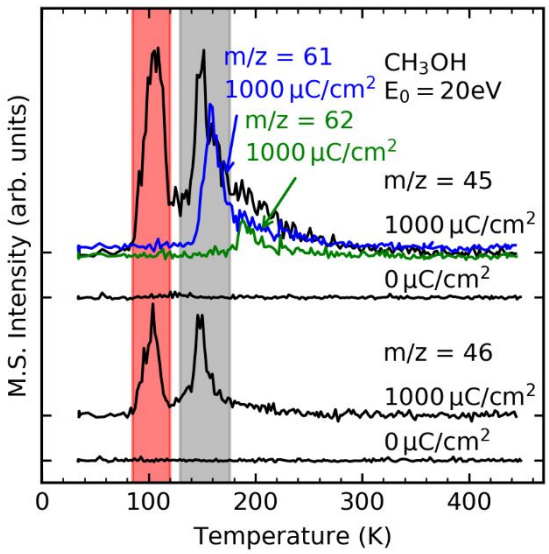

Figure 7. Thermal desorption spectra of a multilayer film of CH_3OH without electron exposure (denoted 0 µC/cm²) and after electron irradiation with 1000 µC/cm² at E_0 = 20 eV. The peaks at 100 and 152 K in the *m/z* = 45 and 46 curves are assigned to CH_3OCH_3 (red) and CH_3CH_2OH (grey), respectively. Note, however, that desorption of CH_3OCH_2OH (blue line) and $HOCH_2CH_2OH$ (green line) contribute to the overall *m/z* = 45 signal as can be seen by the peak positions of the *m/z* = 61 and *m/z* = 62 signals of CH_3OCH_2OH and $HOCH_2CH_2OH$, respectively (see also Figure 5). Tick marks on the vertical axis indicate the baseline level. Tick marks on the left and right axis indicate the vertical offset of the individual curves. The magnification is the same for all curves.

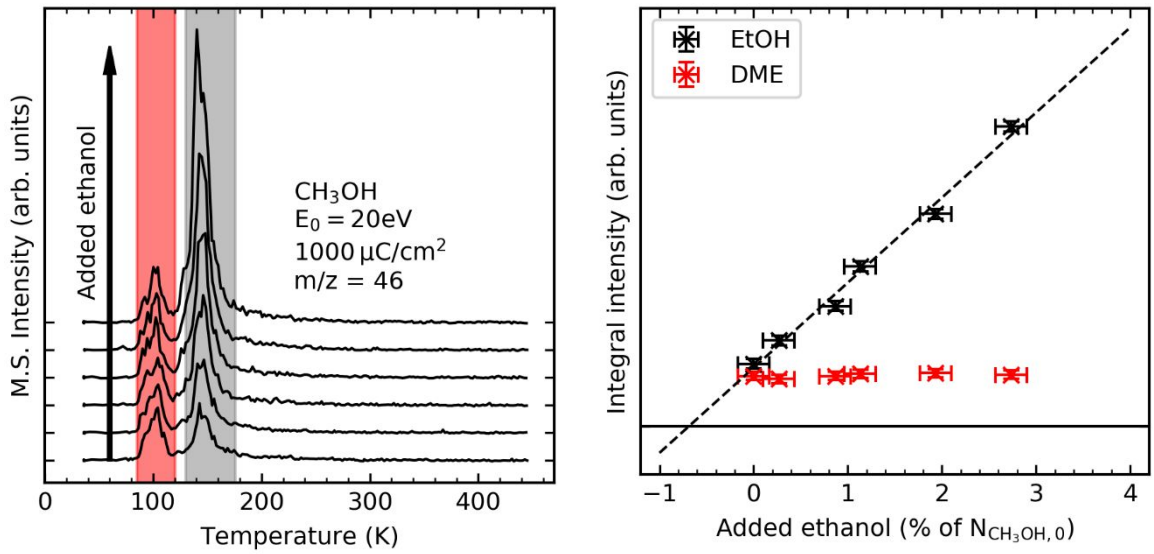

Figure 8. Thermal desorption spectra of a multilayer film of CH_3OH after electron irradiation with 1000 µC/cm² at E_0 = 20 eV (bottom spectrum in left panel). The peaks at 100 K and 152 K in the *m/z* = 46 curves have been assigned to CH_3OCH_3 (DME) and CH_3CH_2OH, (EtOH) respectively. The assignment of the peak at 152 K to CH_3CH_2OH was further verified by condensing increasing amounts of CH_3CH_2OH on top of the irradiated sample (Left panel). This leads to an increase of the peak area for the signal at 152 K (black) while the peak area of the first signal at 100 K (red) remains constant (right panel). Tick marks on the left and right axis of the left panel indicate the vertical offset of the individual curves. The magnification is the same for all curves. The horizontal line in the right panel indicates an integral intensity of zero.

Dependence of Product Yield on Electron Exposure

The depletion of CH_3OH as well as degradation of the products must be negligible in order to compare product yields obtained for different electron energies. Within this regime of initial rates, the product yield increases linearly with electron exposure and formation rates are reflective of formation cross sections. To identify electron exposures that are within the regime of initial rates, we performed irradiation experiments at electron energies of

20 eV with increasing exposures for every product. As an illustrative example, the dependence of the H_2CO yield on electron exposure is shown in Figure 9. The exposure dependence of the other products is shown in Figure S7–S9. Formation of H_2CO was monitored by adding the amounts of H_2CO that desorbed during ESD and TDS. Studies on the electron-induced decomposition of acetone into CH_4 and CO have shown that integrated ESD and TDS signals for specific mass-to-charge ratios can be directly compared.[55] Note that CH_3OH contributes only as a minority species to the *m/z* = 30 ESD signal (Figure 2) suggesting that the integrated *m/z* = 30 signal is roughly reflective of the H_2CO yield that desorbs during electron exposure. On the basis of this analysis, the product yield of H_2CO increases linearly with electron exposure up to 500 μC/cm². At higher electron exposures, the yield of product retained in the film approaches saturation as is deduced from the TDS because degradation of H_2CO and/or depletion of CH_3OH are no longer negligible while the yield of H_2CO that desorbs during ESD still increases.

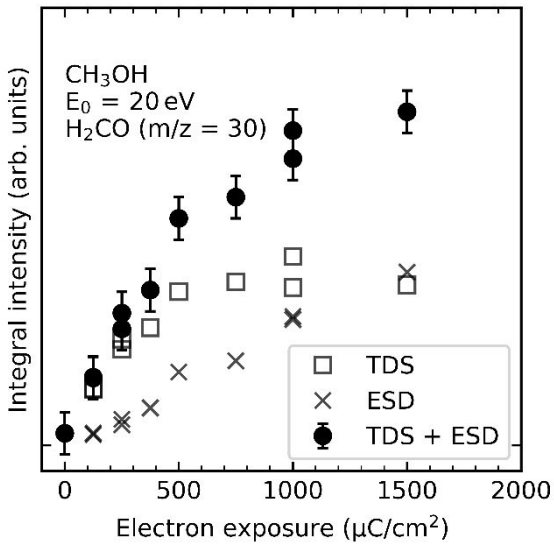

Figure 9. Areas under the *m/z* = 30 desorption signals of H_2CO obtained by ESD (stars) and TDS (squares) after increasing electron irradiation of multilayer films of CH_3OH at E_0 = 20 eV. The sum of ESD and TDS signal areas (filled circles) reflects the overall amount of H_2CO that has been formed. Tick marks on the vertical axis denote an integral intensity of zero. Error bars represent the estimated error for the intergal intensity.

An earlier study on CH_3OH/C_2H_4 mixtures has shown that DEA to CH_3OH at 5.5 eV leads to the formation of ethyl methyl ether.[34] In addition, formation of $HOCH_2CH_2OH$ and CH_3OCH_2OH has been reported to occur by ND at electron energies as low as 6 eV.[3] We thus additionally studied the dependence of H_2CO yield on electron exposures at an electron energy of 5.5 eV in order to account for the possible formation of H_2CO by DEA, and at 8 eV in order to account for the possible formation of H_2CO by ND. Furthermore, the dependences of product yields on electron exposure for CH_4, CH_3CH_2OH, CH_3OCH_3, and CH_3OCH_2OH at 8 eV are shown in Figure S12–S15. No dataset is shown for $HOCH_2CH_2OH$ because of the poor signal-to-noise ratio at lower electron exposures. We assume, however, that $HOCH_2CH_2OH$ shows a similar behaviour as CH_3OCH_2OH,

CH_3CH_2OH, and CH_3OCH_3. At these lower energies, considerably higher exposures are required to obtain any observable signal in the TDS (Figure 10). In contrast to higher energies, no ESD signals have been observed for electron energies below 9 eV. The areas under the TDS signals are thus directly reflective of the overall amounts of products. Both at 5.5 and 8 eV, the H_2CO yield increases linearly up to 9000 μC/cm² before it approaches saturation. This is not surprising since cross sections for DEA, ND, and EI can vary by several orders of magnitudes.[30] In consequence, two sets of irradiation experiments with different electron exposures are necessary to study the energy dependence above and below the ionization threshold of CH_3OH.

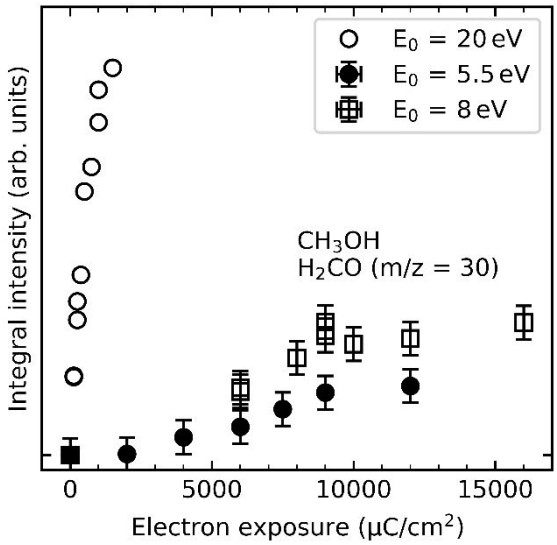

Figure 10. Areas under the *m/z* = 30 desorption signal of H_2CO obtained by TDS after increasing electron irradiation of multilayer films of CH_3OH at E_0 = 5.5 eV (filled circles) and 8 eV (hollow squares). Error bars denote the estimated error for the integral intensity. Product yields obtained at different electron exposures at 20 eV (hollow circles, see Figure 9) are plotted for comparison. Tick marks on the vertical axis mark an integral intensity of zero.

In order to make sure that the approximation of initial rates is valid, we studied the dependence of H_2CO formation on electron energy with electron exposures of 500 μC/cm² in the energy range from 2.5 to 20 eV and with 9000 μC/cm² in the energy range from 2.5 to 9.0 eV. The electron exposures to be used to study the energy dependences of product formation for other products as derived from the electron exposure dependences are compiled in Table 1.

Table 1. Electron exposures, *m/z* values, and integration region used to study the energy dependences of product formation in the range of 2.5–9 eV and 2.5–20 eV.

	Electron exposure used in energy dependence (μC/cm²)		Parameters used for analysis	
Compound	Electron energies 2.5–9 eV	Electron energies 2.5–20 eV	*m/z*	Integration region (K)
H_2CO	9000	500	30	73–105
CH_4	9000	125	16	35–106
CH_3OCH_3	32000	500	46	80–125
CH_3CH_2OH	32000	500	46	135–200
CH_3OCH_2OH	32000	400	61	130–250
$HOCH_2CH_2OH$	32000	400	33	175–250

Dependence of Product Yield on Electron Energy

The yields of CH_4, H_2CO, $HOCH_2CH_2OH$, CH_3OCH_2OH, CH_3OCH_3, and CH_3CH_2OH were monitored at electron energies in the range from 2.5 to 20 eV to reveal the initial electron-molecule interactions that are relevant for the formation of these products. The electron exposure was chosen within the regime of initial rates as deduced from the dependences of product yields on electron exposure (Table 1). At lower electron exposures, product formation is observable with an onset at 9 eV in TDS and, in the cases of H_2CO and CH_4, also in ESD (Figure 11). This energy roughly coincides with the ionization threshold of CH_3OH in the condensed phase which is located at 9.8 eV.[56] ESD has not been observed for $HOCH_2CH_2OH$, CH_3OCH_2OH, CH_3OCH_3, or CH_3CH_2OH (Figure 11). This, however, is not surprising as the efficiency of ESD decreases with molecular mass.[57] Starting from an onset at 9 eV, ESD of CH_4 and H_2CO increases steadily with electron energy which reflects the increasing desorption probability. The majority of CH_4 and H_2CO, however, is retained in the film as can be deduced from the ratio between the areas under the ESD and TDS signals. The overall energy dependences derived by adding the TDS and ESD signal areas (not shown) thus do not deviate qualitatively from those obtained by TDS alone.

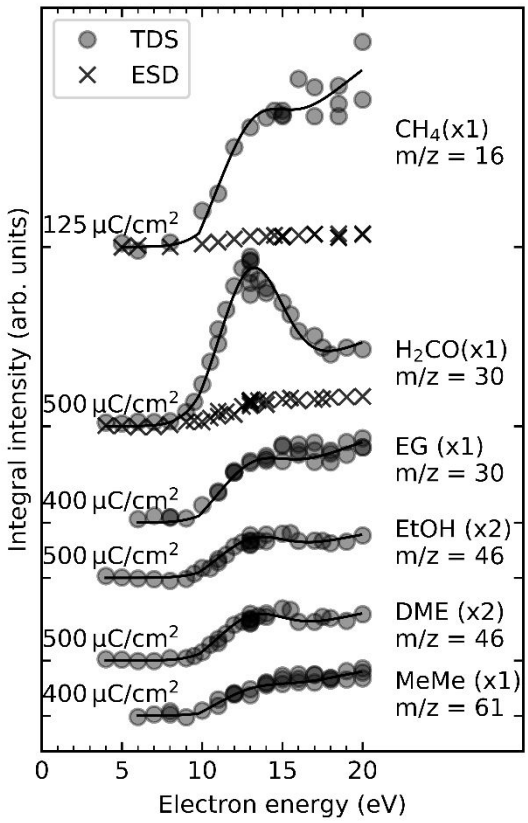

Figure 11. Areas under the *m/z* = 16 signal of CH_4, *m/z* = 30 signal of H_2CO, *m/z* = 33 signal of $HOCH_2CH_2OH$ (EG), *m/z* = 46 signal of CH_3CH_2OH (EtOH), *m/z* = 46 signal of CH_3OCH_3 (DME), and *m/z* = 61 signal of CH_3OCH_2OH (MeMe) obtained by TDS (circles) and ESD (stars) produced during the stated electron exposures of condensed CH_3OH. Error bars were omitted for clarity. The solid lines serve as guide to the eye. Note that no ESD was observed for $HOCH_2CH_2OH$, CH_3CH_2OH, CH_3OCH_3, and CH_3OCH_2OH. Tick marks on the left and right axis indicate the vertical offset of the individual curves. The curves are magnified by the denoted factors.

The energy dependences of H_2CO, CH_4, CH_3CH_2OH, and CH_3OCH_3 show resonances at 13 eV pointing to an initiating DEA process. In contrast, resonant behaviour is less obvious for $HOCH_2CH_2OH$ and CH_3OCH_2OH although minor contributions of this resonance to the overall product yield could explain the plateau-like behavior for energies higher than

13 eV. For electron energies higher than 13 eV, product yields do not decline to baseline level indicating that ND or EI also lead to product formation. The highest energy resonance for the production of anions from CH_3OH has been observed at 10.5 eV in the gas phase[58–60] and at 11.0 eV in the condensed phase.[3] This, however, is considerably lower than the resonance observed in the present study and can thus not be responsible for the formation of products. A similar resonance at 14 eV, however, was observed by Lepage et al.[4] for the production of CO from condensed CH_3OH.

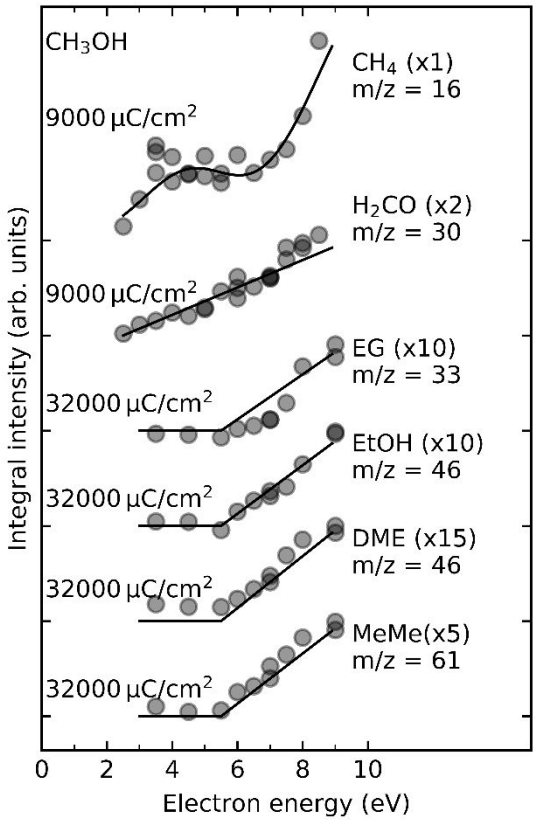

Figure 12. Areas under the *m/z* = 16 signal of CH_4, *m/z* = 30 signal of H_2CO, *m/z* = 33 signal of $HOCH_2CH_2OH$ (EG), *m/z* = 46 signal of CH_3CH_2OH (EtOH), *m/z* = 46 signal of CH_3OCH_3 (DME), and *m/z* = 61 signal of CH_3OCH_2OH (MeMe) obtained from CH_3OH during the stated electron exposures and monitored by TDS. Error bars were omitted for

clarity. The solid lines serve as guide to the eye. Tick marks on the left and right axis indicate the vertical offset of the individual curves. The curves are magnified by the denoted factors.

An additional set of experiments with higher electron exposures was performed to study the formation of products below the ionization threshold (Figure 12). At these lower electron energies, no ESD is observed for any product. Thus, the amounts of products derived from TDS after irradiation directly reflect the overall amounts of these products. Formation of $HOCH_2CH_2OH$, CH_3OCH_2OH, CH_3OCH_3, and CH_3CH_2OH starts from an onset at ~6 eV which is well below the ionization threshold of CH_3OH. The onset, however, roughly coincides with the excitation threshold of CH_3OH which is 6.7 eV in the condensed phase.[61] Starting from this threshold, product yields of $HOCH_2CH_2OH$, CH_3OCH_2OH, CH_3OCH_3, and CH_3CH_2OH increase steadily with increasing electron energies suggesting that ND is responsible for the formation of these products. Noticeably, no resonances are observed for the formation of these products here. This suggests that below the ionization threshold, DEA does not play a role for the formation of these products. Our results thus agree with those of Boyer et al. who did neither observe any resonances for the production of $HOCH_2CH_2OH$ and CH_3OCH_2OH in this energy regime.[3]

In contrast, formation of H_2CO and CH_4 is observable at energies as low as 2.5 eV which is considerably below the excitation threshold of CH_3OH and can thus not be triggerd by ND. The product yield of H_2CO increases steadily with electron energy which is typically more characteristic of a non-resonant process. It is possible, however, that DEA is masked

by the concomitant onset of ND at ~6 eV. In the case of CH_4, a pronounced shoulder at ~5 eV is observed suggesting that DEA is involved in the formation of CH_4. The observed shoulder does not agree well with known DEA resonances of CH_3OH at 6.5 eV in the gas phase and 6 eV in the condensed phase.[3,34,60] Alternatively, the formation of CH_4 at these lower electron energies might be attributed to a resonance yielding $O^{\bullet-}$ between 3 eV and 4 eV which has been observed in condensed phase ESD experiments by Kundu et al.[62] but has not been reported by Boyer et al.[3] For electron energies higher than 7.5 eV, the product yield of CH_4 increases again suggesting that either another resonance, or ND contributes to the production of CH_4. We note that the electron energy dependence of the yields of $HOCH_2CH_2OH$ and CH_3OCH_2OH has been reported before from TDS experiments applying exposures of 1900 $\mu C/cm^2$.[3] Similar to the larger exposure experiments of the present study, this work observed an onset between 6 eV and 7 eV and a continuous increase towards higher energies. Product formation has thus been ascribed to EE processes.

Product yields

Relative molecular abundances of the irradiation products have been obtained from the ESD and TDS data. These can be estimated by comparing the integrated desorption signals and correcting these for the different partial ionization cross sections of the observed fragments. Hereinafter, we state all relative molecular abundances with respect to the initial CH_3OH ice abundance.

In order to test the accuracy of our procedure for deriving product yields, we used the data shown in Figure 6 and Figure 8 where defined amounts of either $HOCH_2CH_2OH$ or CH_3CH_2OH, determined from the pressure drop in the gas handling manifold, were condensed on top of a preirradiated CH_3OH film. This leads to a linear increase of the respective desorption signal with the amount of material deposited on top of the irradiated sample. The amount that was initially present after irradiation is then represented by the intercept of the regression line with the horizontal line that indicates an integral intensity of zero in the left panels of Figure 6 and Figure 8. The uncertainty of the amounts has been calculated from the uncertainty of the intercept which, in turn, has been deduced from the covariance matrix of the linear regression. From those experiments, relative molecular abundances of 1.4 ± 0.3 % for $HOCH_2CH_2OH$, and 0.68 ± 0.08 % for CH_3CH_2OH were obtained. These values agree well with those obtained by comparing the desorption peaks of $HOCH_2CH_2OH$ and CH_3CH_2OH with that of CH_3OH taking into account the partial ionization cross sections of the observed fragments. The latter analysis results in relative abundances of 1.0 ± 0.3 % for $HOCH_2CH_2OH$, and 0.57 ± 0.10 % for CH_3CH_2OH. We thus consider our results as accurate within the error margins.

Integrated desorption signals for electron energies below the ionization threshold were derived from irradiations with electron exposures of 9000 μC/cm² for CH_4 and H_2CO, and with electron exposures of 32000 μC/cm² for $HOCH_2CH_2OH$, CH_3OCH_2OH, CH_3OCH_3, and CH_3CH_2OH. Note that product yields obtained with electron exposures of 32000 μC/cm² are still within the linear regime of initial rates (see Figure S12–S15). In

order to compare product yields obtained after electron exposures of 32000 μC/cm² and 9000 μC/cm², we scaled the product yields of $HOCH_2CH_2OH$, CH_3OCH_2OH, CH_3OCH_3, and CH_3CH_2OH by a factor of 9/32. Our results reveal that below 6 eV, H_2CO and CH_4 are the only products (Figure 12). At E_0 = 8 eV, relative molecular abundances of products are 1.1 ± 0.2 % for CH_4, 0.6 ± 0.1 % for H_2CO, 0.030 ± 0.007 % for $HOCH_2CH_2OH$, 0.04 ± 0.01 % for CH_3OCH_2OH, 0.043±0.008 % for CH_3OCH_3, and 0.07 ± 0.02 % for CH_3CH_2OH (Figure 13, panel A). The value given for CH_3OCH_3 represents a lower limit, as it is based on NIST spectra, rather than mass spectra recorded in our experimental chamber, where we observe slightly lower intensities for higher mass fragments than in NIST reference data. At E_0 = 20 eV, the amounts of products are compared for electron exposures of 250 μC/cm² because this allows us to compare product yields directly without scaling. Our results reveal that the amounts of products as a fraction of initial CH_3OH ice abundance are 1.35 ± 0.20 % for CH_4, 0.55 ± 0.15 % for H_2CO, 0.40 ± 0.13 % for $HOCH_2CH_2OH$, 0.16 ± 0.05 % for CH_3OCH_2OH, 0.06 ± 0.02 % for CH_3OCH_3, and 0.24 ± 0.06 % for CH_3CH_2OH (Figure 13, panel B). Note that the value given for CH_3OCH_3 represent a lower limit due to the reasons mentioned above. From the reported data by Lepage et al.[4], it can be deduced that the relative molecular abundance of CO after irradiation with 250 μC/cm² at 20 eV is about 0.65 % (see Supporting information for calculation). The amount of CO should thus be similar to that of H_2CO in the present study. We note that the loss of CH_3OH during irradiation with 250 μC/cm² at 20 eV amount to roughly 3–5% according to our TDS data (not shown). Considering that the formation of

each of the observed products apart from CH_4, H_2CO, and CO requires two molecules of CH_3OH, the product yields account reasonably for the loss of CH_3OH suggesting that at least the majority of the products have in fact been identified.

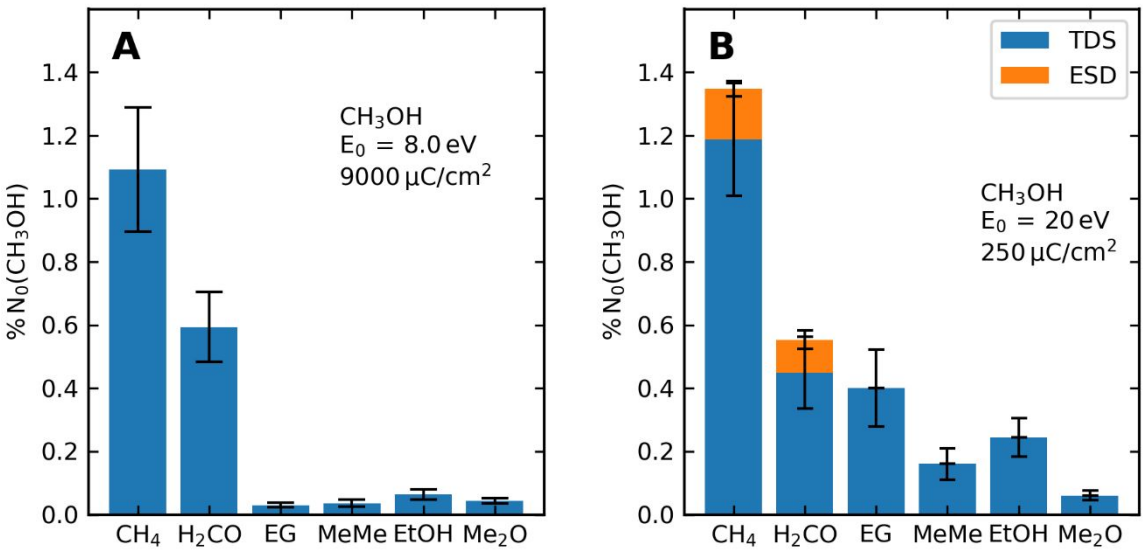

Figure 13. Amounts of CH_4, H_2CO, $HOCH_2CH_2OH$ (EG), CH_3OCH_2OH (MeMe), CH_3CH_2OH (EtOH), and CH_3OCH_3 (Me_2O) in % of the initial CH_3OH ice abundance. (A) Data obtained from TDS after irradiation with 9000 µC/cm² (CH_4 and H_2CO) and 32000 µC/cm² (others) at E_0 = 8 eV, respectively. Abundances of $HOCH_2CH_2OH$, CH_3OCH_2OH, CH_3CH_2OH, and CH_3OCH_3 were scaled by a factor of 9/32 to correct for the higher electron exposures. (B) Data obtained from ESD and TDS after irradiation with 250 µC/cm² at 20 eV, respectively. Note that the values given for CH_3OCH_3 represent lower limits. Error bars denote the estimated uncertainty of amounts.

Discussion of the Reaction Mechanism

Overview of Electron-Methanol Interactions

In order to unravel the reaction mechanisms leading to the observed products, it is necessary to identify the reactive species produced by electron-molecule interactions and to understand their subsequent chemistry. In the investigated CH_3OH ices, the initial interaction of an electron with CH_3OH can yield $CH_3OH^{\bullet+}$, CH_3OH^*, and $CH_3OH^{\bullet-}$ after EI, EE, and EA, respectively.The ionization threshold in the gas phase is 10.84 eV and is lowered to ~9.8 eV in the condensed phase because of polarization effects.[46,56] In the gas phase, fragmentation of CH_3OH by DI already sets in at electron energies of 10.6 ± 0.5 eV and thus almost coincides with the ionization threshold.[63] Experiments with CH_3OH clusters, however, suggest that the $CH_3OH^{\bullet+}$ radical cation is in fact stabilized in the condensed phase by neighbouring molecules which largely suppresses fragmentation.[64,65] We thus propose that DI does not play a significant role in the condensed molecular films studied herein. The thresholds for EE of CH_3OH are ~6.4 eV in the gas phase and 6.7 eV in the condensed phase.[61,66] Following EE of CH_3OH, ND might produce a variety of fragments by single-bond and/or multi-bond cleavages. Unfortunately, experimental data on the fragmentation dynamics of CH_3OH by ND following electron impact, i.e., the kind of formed fragments, their formation thresholds, and formation cross sections are very sparse. Dech et al. reported a threshold of 13 eV for the production of $O(^1S)$ in crossed beam experiments.[67] From thermodynamic considerations, the authors concluded that $O(^1S)$ is likely formed by decomposition of

CH_3OH into $CH_3^{\bullet}$, $H^{\bullet}$, and $O(^1S)$. Furthermore, Donohue et al. reported the thresholds for several excited fragments of CH_3OH of which only the thresholds for the production of $HO(A^2)$ at 10.1 eV and that of $CH(A^2)$ at 13.2 eV might be relevant in the present study as other excited fragments are not formed below 20 eV.[68] To our knowledge, thresholds have not been reported for the production of ground state fragments which are especially relevant for chemical reactions below the ionization threshold of CH_3OH. However, as optically allowed channels are typically dominant in electron-molecule interactions, important informations on these unknown properties might also be inferred from studies on photochemistry. Its is known that UV irradiation of condensed CH_3OH at 157 nm (7.9 eV) leads to single bond cleavages yielding $^{\bullet}CH_2OH$, $CH_3O^{\bullet}$, $H^{\bullet}$, $HO^{\bullet}$, and $CH_3^{\bullet}$ radicals as well as to elimination of H_2 yielding HCOH and H_2CO.[69–71] Unimolecular photodissociation of CH_3OH into CH_4 and $O(^1D/^3P)$, on the other hand, has not been observed.[69] As EE equally proceeds via electronically excited neutral states, we propose that ND of CH_3OH produces the same fragments as photodissociation. Finally, DEA to CH_3OH is known to produce CH_3O^-, H^-, and $O^{\bullet-}$ (Table 3), as well as the corresponding neutral species.[3]

Table 2. Anions and resonance energies observed for DEA to CH_3OH in the gas and condensed phase.

	resonance energies (eV)	
fragment	gas Phase	condensed phase
CH_3O^-	2.9[a]	

	6.5[a, b] 8.0[a, b] 10.5[a, b]	8.8[c] 11.5[c]
H^-	6.5[a, d] 8.0[a, d] 10.5[a, d]	6[c] (shoulder) 7.8[c]
$O^{\bullet-}$	7 (weak)[b] 10.5[a, b]	3–4[e] 8.0[c] 11.0[c]

References: [a]Ibănescu et al.[60], [b]Kühn et al.[58],[c]Boyer et al.[3], [d]Curtis and Walker[59], [e]Kundu et al.[62].

In addition, a resonance at 14 eV was observed in the yields for the electron-induced formation of CO from condensed CH_3OH.[4] Lepage et al. attributed this resonance to EA yielding $CH_3OH^{\bullet-}$, which quickly decays into electronically excited CH_3OH^* (reaction 1) leading to subsequent dissociation into smaller fragments of which only CO has been monitored.[4]

$$\mathrm{CH_3OH + e^-(E_0) \rightarrow CH_3OH^{\bullet-} \rightarrow CH_3OH^* + e^-(E')} \quad (1)$$

Thus, no ionic fragments are produced which is the reason why this resonance has not been observed in ESD[3] and in crossed-beam experiments.[58,72]

Reactive species produced by the initial electron-molecule interactions described so far can then react with neighbouring CH_3OH molecules or migrate through the ice film until

they encounter other reactive species. For instance, HO^-, CH^-, CH_2^- and CH_3^- were observed, in addition to the products seen in gas phase DEA, in ESD from condensed CH_3OH.[3] It was shown that these species are not produced directly by decay of the TNI but by ion-molecule interactions of $O^{\bullet-}$ and H^- with CH_3OH.[3] This underlines that a comprehensive understanding of the possible ion-molecule, radical-molecule, and radical-radical reactions is essential to unravel reaction mechanisms that underly the formation of the stable products formed upon electron irradiation of condensed CH_3OH.

From EI of CH_3OH clusters, it is known that the $CH_3OH^{\bullet+}$ radical cation is a strong acid that can transfer one of its protons to a neighbouring CH_3OH molecule yielding $CH_3OH_2^+$, and a $CH_3O^\bullet$ or $^\bullet CH_2OH$ radical (reactions 2 and 3).[64,65]

$$CH_3OH^{\bullet+} + CH_3OH \rightarrow CH_3OH_2^+ + CH_3O^\bullet \quad (2)$$

$$CH_3OH^{\bullet+} + CH_3OH \rightarrow CH_3OH_2^+ + {}^\bullet CH_2OH \quad (3)$$

In those cluster experiments, the $CH_3OH_2^+$ cation has been reported to undergo a nucleophilic displacement reaction with a nearby CH_3OH molecule yielding CH_3OCH_3 and H_2O (see also “Reactions Leading to Molecular Synthesis”).[64,65]

Considering next ion-molecule reactions induced by DEA, the ions H^-, $O^{\bullet-}$, and CH_3O^- can be involved. The reactivity of $O^{\bullet-}$ has been reviewed comprehensively by Lee and Grabowski.[73] The $O^{\bullet-}$ radical anion is a fairly strong base but can also act as radical. Reaction of $O^{\bullet-}$ with CH_3OH yields HO^- and $CH_3O^\bullet$ as well as smaller amounts of HO^- and $^\bullet CH_2OH$, and $HO^\bullet$ and CH_3O^- according to reactions 4–6.[73]

$$O^{\bullet-} + CH_3OH \rightarrow HO^- + CH_3O^{\bullet} \quad (4)$$

$$O^{\bullet-} + CH_3OH \rightarrow HO^- + {}^{\bullet}CH_2OH \quad (5)$$

$$O^{\bullet-} + CH_3OH \rightarrow HO^{\bullet} + CH_3O^- \quad (6)$$

The ion-molecule reactions of H^- with CH_3OH, in contrast, mainly leads to a proton transfer yielding H_2 and CH_3O^-.[74]

$$H^- + CH_3OH \rightarrow H_2 + CH_3O^- \quad (7)$$

H_2 is not kept in the film and will thus not participate in subsequent reactions. The HO^- anion is a strong base and can thus undergo proton transfer with CH_3OH yielding CH_3O^- and H_2O, respectively.

$$HO^- + CH_3OH \rightarrow H_2O + CH_3O^- \quad (8)$$

This reveals that ion-molecule reactions following EI and DEA mainly lead to the formation of smaller products and radicals. In particular, they fail to explain the observed formation of more complex molecule with the exception of CH_3OCH_3. This suggests that radical-molecule and radical-radical reactions must be responsible for the formation of the more complex molecules. Noticeably, the required radicals for those reactions are not only produced by ND but also by EA, DEA and EI either directly or as a consequence of the ion-molecule reactions discussed above. Addition reactions of radicals that would form larger products are limited to compounds that have multiple bonds such as C_2H_4 or CO.[34,75] Reactions between a radical and a saturated compound, on the contrary, typically

lead to hydrogen abstraction.[76] Therefore, it can be expected that radical-molecule reactions between CH_3OH and $CH_3^{\bullet}$, $HO^{\bullet}$, $CH_3O^{\bullet}$ or $^{\bullet}CH_2OH$ radicals yield CH_4, H_2O, and CH_3OH, respectively, as well as a new $CH_3O^{\bullet}$ or $^{\bullet}CH_2OH$ radical. Unsaturated co-products of electron irradiation like H_2CO and CO, however, might also participate in subsequent radical-molecule reactions if their concentration is sufficiently high. Finally, reactions between two radicals can lead to either disproportionation (reaction 9) or recombination (reaction 10). In both cases, closed-shell molecules are produced which are typically stable.

$$\mathrm{HR}^{\bullet} + \mathrm{HR}'^{\bullet} \rightarrow \mathrm{R} + \mathrm{H_2R}' \tag{9}$$

$$\mathrm{R}^{\bullet} + \mathrm{R}'^{\bullet} \rightarrow \mathrm{R} - \mathrm{R}' \tag{10}$$

As the number of possible radical-radical reactions increases drastically with the number of radical species, the reaction network can become quite complex. However, the energy dependences of $HOCH_2CH_2OH$, CH_3OCH_2OH, CH_3OCH_3, and CH_3CH_2OH are highly correlated suggesting that the same electron-molecule interactions are responsible for their formation. We therefore start by discussing those reactions that lead to molecular synthesis in the sense that larger products are formed from smaller parent compounds (see “Reactions Leading to Molecular Synthesis”). In contrast, H_2CO and CH_4 show rather unique energy dependences. The formation of these two products is thus discussed separately in the sections entitled “Reactions Leading to Formaldehyde” and “Reactions Leading to Methane”.

Reactions Leading to Molecular Synthesis

$HOCH_2CH_2OH$, CH_3OCH_2OH, CH_3OCH_3, and CH_3CH_2OH must be formed from two CH_3OH moieties since their molecular mass is higher than that of CH_3OH. In CH_3OH clusters, $CH_3OH_2^+$ cations are formed as a consequence of proton transfer from $CH_3OH^{\bullet+}$, produced by EI of CH_3OH, to a neighbouring CH_3OH molecule. Subsequent reaction between $CH_3OH_2^+$ and an intact CH_3OH molecule can yield protonated CH_3OCH_3 and H_2O.[64,65] Finally, another proton transfer from protonated CH_3OCH_3 to a neighbouring molecule yields neutral CH_3OCH_3 and $CH_3OH_2^+$ (Scheme 1) which results in a chain reaction as the latter can again enter the reaction sequence. Noticably, cluster experiments have not revealed any other products than CH_3OCH_3 and H_2O.[64,65]

Our data show that CH_3OCH_3 is formed in rather low quantities compared to $HOCH_2CH_2OH$, CH_3OCH_2OH, and CH_3CH_2OH (Figure 13). We thus suppose that the chain-reaction in Scheme 1 does not contribute significantly to the product yield of CH_3OCH_3 in the present stuy.

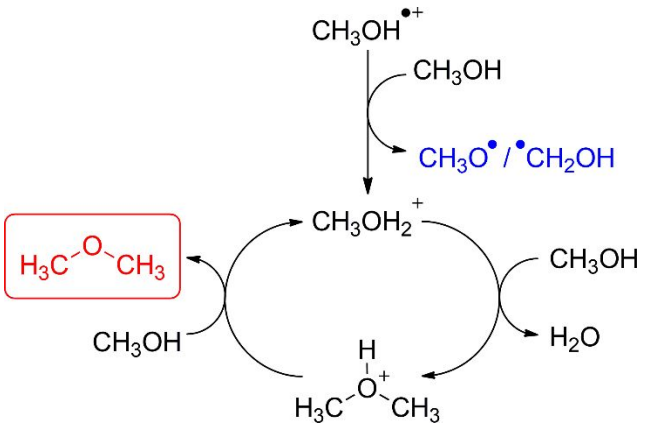

Scheme 1. Mechanism for electron-induced formation of CH_3OCH_3 in CH_3OH clusters. Above the ionization threshold of CH_3OH, a $CH_3OH^{\bullet+}$ radical cation is formed by EI, which can transfer a proton to a nearby CH_3OH molecule yielding $CH_3OH_2^+$ and either $CH_3O^\bullet$ or $^\bullet CH_2OH$ (blue). The $CH_3OH_2^+$ cation is subsequently attacked by the oxygen lone pair of another CH_3OH molecule leading to the formation of protonated CH_3OCH_3 and H_2O. Finally, another proton transfer to a nearby CH_3OH molecule yields neutral CH_3OCH_3 (red) and $CH_3OH_2^+$.[64,65] The latter can again enter the reaction sequence which results in a chain reaction.

In contrast to the relatively small CH_3OH clusters, however, reactions of radicals or ions in the condensed phase are not limited to molecules in the vicinity as they can diffuse through the solid ice and encounter product molecules or other reactive species at a different site. Maity et al. observed that methyl formate and glycolaldehyde are formed much more efficiently in CO/CH_3OH (1:1) ice mixtures than in pure CH_3OH ice.[10] This suggests that co-products like CO might undergo radical-molecule reactions and thus contribute to the overall product yields. Similarly, H_2CO might be involved in the formation of $HOCH_2CH_2OH$, CH_3OCH_2OH, CH_3CH_2OH, and CH_3OCH_3. We did, however, not observe higher product yields upon electron-irradiation of H_2CO/CH_3OH (1:100–3:100)

mixtures compared to films of pure CH_3OH (not shown) indicating that reactions between radicals and the co-product H_2CO are negligible in the present study.

The most cited mechanism for the production of $HOCH_2CH_2OH$, CH_3OCH_2OH, CH_3CH_2OH, and CH_3OCH_3 is ND of CH_3OH into $CH_3O^{\bullet}$, $^{\bullet}CH_2OH$, and $CH_3^{\bullet}$ radicals followed by recombination among these species.[2,3,7,16,18] $HOCH_2CH_2OH$ is formed by recombination of two $^{\bullet}CH_2OH$ radicals, CH_3OCH_2OH is formed by recombination of $^{\bullet}CH_2OH$ and $CH_3O^{\bullet}$, CH_3OCH_3 is formed by recombination of $CH_3O^{\bullet}$ and $CH_3^{\bullet}$ radicals, and CH_3CH_2OH is formed by recombination of $^{\bullet}CH_2OH$ and $CH_3^{\bullet}$ radicals (Scheme 2).

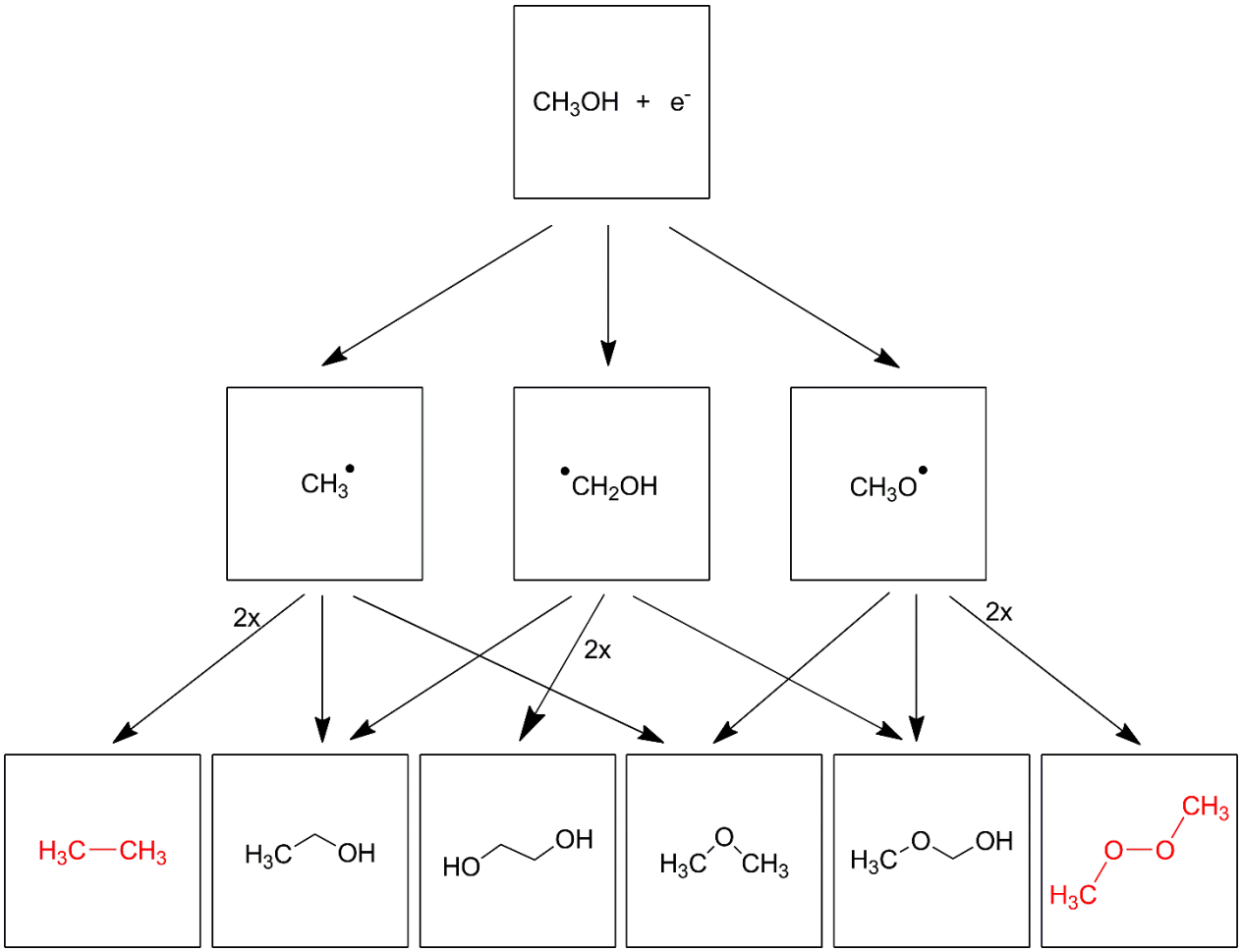

Scheme 2. Electron-molecule interactions lead to the formation of $CH_3^{\bullet}$, $^{\bullet}CH_2OH$, and $CH_3O^{\bullet}$ radicals which can recombine to yield $HOCH_2CH_2OH$, CH_3OCH_2OH, CH_3OCH_3, and CH_3CH_2OH. The potential recombination products ethane (C_2H_6) and dimethyl peroxide (CH_3OOCH_3) (red) have not been observed in the present study.

Statistical recombination among those radicals should also yield dimethyl peroxide (CH_3OOCH_3) by recombination of two $CH_3O^{\bullet}$ moieties and ethane (C_2H_6) by recombination of two $CH_3^{\bullet}$ moieties. To our knowledge, formation of CH_3OOCH_3 has been reported in only one publication[14] where experiments have been performed with a more sensitive mass spectrometer as well as with much higher film thicknesses. In the present study, we do not observe CH_3OOCH_3 as has been inferred by the absence of a second

signal in the *m/z* = 62 curve of the TDS beside that of $HOCH_2CH_2OH$. We thus suppose that the amount of CH_3OOCH_3 formed in the present study is below the detection limit of the QMS.

To our knowledge, C_2H_6 has not been found in any study.[2,6,7,9,11,16,17] Studies by Öberg et al. revealed that at lower temperatures, $CH_3^\bullet$ is more mobile than $CH_3O^\bullet$ and $^\bullet CH_2OH$ radicals. Therefore, they ascribed the absence of C_2H_6 to a higher abundance of $^\bullet CH_2OH$ and $CH_3O^\bullet$ radicals compared to $CH_3^\bullet$ which makes reactions between $CH_3^\bullet$ and $CH_3O^\bullet$, and $CH_3^\bullet$ and $^\bullet CH_2OH$ more likely than recombination of two $CH_3^\bullet$ moieties.[16] In agreement with earlier publications, we did not find any evidence for the formation of C_2H_6 in the present study either. Our data, however, indicate that $CH_3^\bullet$ radicals are present in sufficient abundance so that CH_3CH_2OH is produced in higher yields than, for instance, CH_3OCH_2OH, which is formed by recombination of $CH_3O^\bullet$ and $^\bullet CH_2OH$. This implies that rapid trapping of $CH_3^\bullet$ causes the higher abundance of $CH_3O^\bullet$ and $^\bullet CH_2OH$. Noticeably, this effect includes not only recombination with other radicals but is most likely enhanced by the reaction of $CH_3^\bullet$ with a nearby CH_3OH molecule, which yields CH_4 and either $CH_3O^\bullet$ or $^\bullet CH_2OH$. The latter type of reaction lowers the effective concentration of $CH_3^\bullet$ radicals in the ice but increases that of $CH_3O^\bullet$ and $^\bullet CH_2OH$ (see also “Reactions Leading to Methane”), in line with the interpretation by Öberg.[16]

We conclude that radical recombination is the dominant mechanism responsible for the formation of $HOCH_2CH_2OH$, CH_3OCH_2OH, CH_3OCH_3, and CH_3CH_2OH in the present

study and that ion-molecule and radical-molecule reactions are negligible. Our data suggest, however, that the required radicals are not only formed by ND but also by EI or EA with subsequent autodetachment. The energy dependences of product yields suggest that below the ionization threshold of CH_3OH, ND is the only electron-molecule interaction that produces the radicals necessary for product formation. In analogy to photofragmentation at a wavelength of 157 nm, we propose that ND following electron impact yields $CH_3^{\bullet}$, $CH_3O^{\bullet}$, and $^{\bullet}CH_2OH$ radicals.[69–71]

The presence of a second onset at ~9 eV, which coincides roughly with the ionization threshold of CH_3OH, suggests that EI also plays a role at energies above the ionization energy of CH_3OH. We propose that this is due to the proton transfer from $CH_3OH^{\bullet+}$ to a neighbouring CH_3OH molecule which produces $CH_3O^{\bullet}$ and $^{\bullet}CH_2OH$ radicals (reactions 2 and 3).

Furthermore, the energy dependences of CH_3CH_2OH and CH_3OCH_3 show a resonant behaviour at 13–15 eV although not as pronounced as for the formation of H_2CO. In contrast, resonant behaviour is not as obvious in the energy dependences of $HOCH_2CH_2OH$ and CH_3OCH_2OH, but the plateau-like behaviour of product yields for electron energies above 13 eV suggest that there might be minor contributions of EA to the yields of these products as well. We thus propose that EA to CH_3OH followed by autodetachment, as proposed as explanation for CO formation,[4] contributes to some

extent the formation of CH_3OCH_3 and CH_3CH_2OH, and possibly also the formation of $HOCH_2CH_2OH$ and CH_3OCH_2OH.

Reactions Leading to Formaldehyde

At electron exposures of 500 μC/cm², H_2CO formation shows an onset at 9 eV and a resonance at 13 eV (Figure 11). At E_0 = 13 eV, we further observed desorption of H_2 during electron irradiation (Figure S16**Error! Reference source not found.**). Noticeably, the on-resonance formation of H_2CO occurs in the same range of energies as observed by Lepage et al. for the production of CO in condensed CH_3OH that is thought to proceed via reaction 1.[4] We thus propose that the on-resonance formation of H_2CO proceeds by EA to CH_3OH followed by autodetachment and subsequent dissociation of CH_3OH into H_2CO and H_2.

Noticeably, product yields do not decline to baseline level for E_0 > 13 eV indicating that EI and/or ND also lead to formation of H_2CO at these higher energies. Both EI (reactions 2 and 3) as well as ND are known to produce $^{\bullet}CH_2OH$ and $CH_3O^{\bullet}$ radicals. It is conceivable that these radicals split off a $H^{\bullet}$ atom in a unimolecular process to produce H_2CO. However, a previous study has shown that H_2CO formation from $CH_3O^{\bullet}$ produced by an electron-induced reaction of CH_3OH is considerably enhanced in the presence of C_2H_4 which can act as hydrogen acceptor.[34] This suggests that, if at all, only a minor fraction of $CH_3O^{\bullet}$ radicals is able to undergo spontaneous C–H cleavage to form H_2CO. In addition, H_2CO might be produced by hydrogen transfer between either $^{\bullet}CH_2OH$ or $CH_3O^{\bullet}$ and any

other radical R•. We thus conclude that this disproportionation reaction is the more plausible scenario for the formation of H_2CO as observed here.

Disproportionation among radicals that would yield H_2CO competes with recombination that would yield the larger products as discussed in “Reactions Leading to Molecular Synthesis”. However, the relative yield of H_2CO as compared to the larger products is considerably higher at 13 eV where the resonant channel is open than at 20 eV (Figure 11). This suggests that the resonant pathway proposed by Lepage[4] in fact predominantly leads to elimination of H_2 and not to radical formation. In reverse, it also supports the conclusion drawn in “Reactions Leading to Molecular Synthesis” that ND and to some extent EI channels dominate the formation of the the larger products.

At higher electron exposures of 9000 μC/cm², H_2CO formation is observable down to electron energies as low as 2.5 eV (Figure 12) which is considerably below the ionization and excitation thresholds of the parent CH_3OH molecule.[56,66] This suggests that DEA initiates the product formation at these low energies. CH_3OH has known resonances at 2.9 eV, 6.5 eV, 8.0 eV and 10.5 eV in the gas phase, while in condensed phase ESD experiments, resonances have been observed at 3–4 eV, 6 eV, 8–9 eV, and 11 eV (Table 2). The lowest two resonances can contribute to the formation of H_2CO in the low-energy regime.

It is remarkable that larger products are not formed below 6 eV. This finding can be rationalized by a more selective formation of $CH_3O^{\bullet}$ as the radical species that act as

precursors to H_2CO. In this scenario, only two radical reactions are possible, namely recombination among $CH_3O^{\bullet}$ radicals yielding CH_3OOCH_3 and disproportionation to CH_3OH and H_2CO as products.

The DEA resonance at 6.5 eV in the gas phase and at 6 eV in the condensed phase has been reported to yield mainly H^-. From gas phase experiments with isotopically labelled CH_3OH, it is further known that H^- stems exclusively from the –OH group which yields $CH_3O^{\bullet}$.[59] In the condensed phase, negative ion ESD experiments have suggested that H^- stems from both the –OH and $–CH_3$ moiety which would lead to both $CH_3O^{\bullet}$ and $^{\bullet}CH_2OH$ radicals.[77] This interpretation, however, must be treated with caution as the reaction between H^- or D^- with neighbouring CH_3OH molecules can lead to isotopic exchange. This might have occurred in the ESD experiment[77] because CH_3OH molecules tend to form hydrogen bonds to each other leading to clustering even at low coverage.

Similarly, the DEA resonance at 3–4 eV, yielding the $O^{\bullet-}$ radical anion, could in principle produce $CH_3O^{\bullet}$ and $^{\bullet}CH_2OH$ radicals by reaction of $O^{\bullet-}$ with a neighbouring CH_3OH molecule (reaction 4 and 5). Experimental studies suggest, however, that the production of $CH_3O^{\bullet}$ is favoured over that of $^{\bullet}CH_2OH$[73] which again explains the lack of larger recombination products in this energy range as observed in the present study.

In principal, it is also conceivable that H_2CO is formed by elimination of H_2 from CH_3OH which would equally explain the absence of any recombination products below the excitation threshold. From an energetic point of view, this reaction might in fact occur as,

according to our calculations, the difference in Gibbs Free Energy of this process at 35 K is ΔG = +0.20 eV and thus below the onset we observed in the energy dependence of H_2CO. It is, however, not obvious how such a reaction can be initiated below the energetic threshold for ND and EI. In the field of photochemistry, dissociation of CH_3OH with photon energies below the excitation threshold is known to occur upon multiphoton absorption.[78] Multiphoton absorption, however, yields mainly radical species and unimolecular elimination of H_2 does not occur or is at least inefficient.[78] We thus do not believe that multiple vibrational excitation of a CH_3OH molecule by interaction with the impinging electrons is a straightforward explanation for the observed formation of H_2CO below the excitation threshold.

The observed linear increase of H_2CO yield is thus ascribed to overlapping contributions of the DEA resonances at 3–4 eV and at 6 eV as well as of ND starting from an onset at ~6 eV.

Reactions Leading to Methane

The energy dependence of CH_4 formation at electron exposures of 125 μC/cm² reveals an onset at 9 eV which is similar to that of $HOCH_2CH_2OH$, CH_3OCH_2OH, CH_3OCH_3, and CH_3CH_2OH but also shows contributions of a resonant process around 13 eV (Figure 11). As mentioned above, DI of CH_3OH is largely surpressed in the condensed phase. It is thus not obvious, how EI can yield CH_4, because the C–O bond must be cleaved. Therefore, we propose that EE, EA with subsequent autodetachment, or both are

responsible for the production of CH_4 seen in the low-exposure regime as both produce electronically excited CH_3OH molecules. On the basis of kinetic fits, it has been proposed that CH_3OH decays in a unimolecular reaction into CH_4 and $O(^1D)$.[7] To our knowledge, however, this fragmentation channel has not been reported upon electron irradiation in any study. Furthermore, this dissociation channel has been reported to not occur upon photofragmentation of CH_3OH.[69] Since kinetic fits do not allow to infer unambiguous information on a reaction mechanism, we conclude that there is lack of clear evidence for this mechanism in the present study.

In contrast, we have clear evidence for the formation of $CH_3^\bullet$ radicals upon electron irradiation at 20 eV as has been shown by the deconvolution of the ESD integral intensities (see Figure 2). In addition, we have shown that CH_3CH_2OH and CH_3OCH_3 are formed as co-products (Figure 7) which are associated with the production of $CH_3^\bullet$ radicals (Scheme 2). We thus propose that CH_4 is formed by a number of two-step reaction pathways where the first step in each case is the dissociation of the electronically excited CH_3OH into $CH_3^\bullet$ and $HO^\bullet$ radicals (reaction 11) where the initial excitation can be either resonant at energies around 13 eV or direct.

$$\mathrm{CH_3OH + e^-(E_0) \rightarrow CH_3OH^* + e^-(E') \rightarrow CH_3^\bullet + HO^\bullet + e^-(E')} \quad (11)$$

$$\mathrm{CH_3^\bullet + CH_3OH \rightarrow CH_4 + CH_3O^\bullet} \quad (12)$$

$$\mathrm{CH_3^\bullet + CH_3OH \rightarrow CH_4 + {}^\bullet CH_2OH} \quad (13)$$

$$CH_3^{\bullet} + H^{\bullet} \rightarrow CH_4 \quad (14)$$

$$CH_3^{\bullet} + RH^{\bullet} \rightarrow CH_4 + R \quad (15)$$

The initially released $CH_3^{\bullet}$ radical can abstract a $H^{\bullet}$ atom from a nearby CH_3OH molecule (reactions 12 and 13), recombine with a $H^{\bullet}$ atom (reaction 14), or undergo disproportionation with any other radical $RH^{\bullet}$ which leads to the formation of CH_4 (reaction 15). Reactions 12–15 can contribute to the effective lowering of the concentration of these $CH_3^{\bullet}$ radicals proposed in "Reactions Leading to Molecular Synthesis" as reason for the absence of C_2H_6 formation. On the basis of our experimental data, we cannot clearly deduce branching ratios between the different reaction channels. However, based on the excess of CH_3OH present in the reaction mixture, we propose that, above the ionization threshold, CH_4 is predominantly formed by reaction of $CH_3^{\bullet}$ with a nearby CH_3OH (reactions 12 and 13).

The dependence of CH_4 yield on electron energy after electron exposures of 9000 μC/cm² shows an onset for product formation at 2.5 eV and a pronounced shoulder between 4 and 7 eV suggesting an underlying resonant process. We propose that the on-resonance formation of CH_4 around 4 eV proceeds via reaction 16 and is due to the DEA channel yielding $O^{\bullet-}$ reported previously to proceed around 3–4 eV.[62]

$$CH_3OH^{\bullet-} \rightarrow CH_4 + O^{\bullet-} \quad (16)$$

In fact, the fragmentation described by reaction 16 is the only DEA channel leading to $O^{\bullet-}$ that is thermodynamically accessible in this energy range[3,58,59] with the predicted

thermodynamic threshold of 2.4 eV coinciding well with the onset of CH_4 formation in the present work. The additional onset for CH_4 formation at E_0 ~ 7.5 eV roughly coincides with the excitation threshold of CH_3OH. We thus propose that ND of CH_3OH yields $CH_3^{\bullet}$ and $HO^{\bullet}$ radicals, the first of which subsequently react with a nearby CH_3OH molecule to yield CH_4 and either $CH_3O^{\bullet}$ or $^{\bullet}CH_2OH$ (reactions 12 and 13). In addition, the onsets of the higher energy $O^{\bullet-}$ resonances (Table 2) might also contribute to the further increase of CH_4 yield as they produce either intact CH_4 or $CH_3^{\bullet}$ radicals.

Conclusion

The formation of CH_4, H_2CO, $HOCH_2CH_2OH$, CH_3OCH_2OH, CH_3OCH_3, and CH_3CH_2OH in condensed multilayer adsorbates of CH_3OH upon electron irradiation has been monitored by the combined use of electron-stimulated and thermal desorption experiments. The energy dependences of the yields were simultaneously measured for all products between 2.5 eV and 20 eV. From this, reaction mechanisms leading to each product have been deduced. In particular, the close agreement between the energy dependences of the yields of $HOCH_2CH_2OH$, CH_3OCH_2OH, CH_3OCH_3, and CH_3CH_2OH together with the characteristic thresholds behaviour indicates that these products predominantly result from recombination of $CH_3^{\bullet}$, $CH_3O^{\bullet}$ and $^{\bullet}CH_2OH$ radicals that are formed by ND or, above the ionization threshold, by EI and subsequent proton transfer to an adjacent CH_3OH. Radical chemistry also contributes to the non-resonant formation of CH_4 by reaction of a $CH_3^{\bullet}$ radical with a nearby CH_3OH molecule.

In contrast, the formation of H_2CO and, to a smaller extent, also of CH_4 is resonantly enhanced around 13 eV. This process conincides with the previously reported resonant production of CO which was ascribed to EA and subsequent rapid autodetachment that leaves CH_3OH in a highly excited electronic state.[4] This neutral reactive intermediate state most likely decays directly to H_2CO by loss of H_2. Most interestingly, another resonant channel is clearly visible around 4 eV in the energy dependent yield of CH_4. This reaction must be initiated by DEA to CH_3OH which yields $O^{\bullet-}$ as observed previously around 3–4 eV by ESD.[62] From thermodynamic arguments, $O^{\bullet-}$ formation at such low energies can only be realized together with CH_4. The same resonance also accounts for the onset of H_2CO formation near 2.5 eV. The lack of larger products in this energy range is explained by the formation of $CH_3O^{\bullet}$ as the only radical species upon reaction of $O^{\bullet-}$ with CH_3OH. Upon encounter, two $CH_3O^{\bullet}$ radicals can then disproportiate to yield H_2CO and recover one molecule of CH_3OH.

Our results constitute the most comprehensive study of the energy dependence of product formation during electron exposure of condensed CH_3OH reported so far. Together with previous studies on the electron-induced formation of CO[4] as well as $HOCH_2CH_2OH$ and CH_3OCH_2OH[3] from condensed CH_3OH, our study provides a comprehensive picture of the reactions triggered by electron impact with energies in the range between 2.5 eV and 20 eV as representative of low-energy secondary electrons released from condensed material, for instance, under the effect of cosmic radiation. Our results reveal that not only ND, but also DEA as well as EI contribute to the overall product yield which might help to

refine current astrochemical models. We note, however, that DEA to CH_3OH might be underestimated in the present as well as in previous studies as most of the larger recombination products depend on the production rates of two different radical species. Thus, selective dissociation channels yielding specific radicals might not be reflected in the energy dependences of these recombination products. This hypothesis needs to be investigated more comprehensively in future studies. This could be achieved, for example, by mixing CH_3OH with additives like CO that are capable of reacting with specific radicals produced by DEA to CH_3OH.

In contrast to IR spectroscopy, ESD and TDS do not allow to track the temporal evolution of products during irradiation or upon annealing. This drawback, however, is counterbalanced by the high sensitivity of mass spectrometry and the possibility to identify products by specific fragments which are often more characteristic than absorption bands. Thus, both methods provide complementary information that can be used to obtain a more comprehensive picture.

Associated Content

Supporting Information

Figure S1–S2, Thermal desorption spectra for various amount of deposited CH_3OH which were used for monolayer calibration; Figure S3, Mass spectra used to identify characteristic mass-to-charge ratios for the discussed products; Figure S4, ESD spectra used for the integrated signals in Figure 2; Figure S5, Identification of CO; Figure S6,

Identification of methyl formate and glycolaldehyde; Figure S7–S11, dependence of the formation of CH_4, CH_3CH_2OH, CH_3OCH_3, $HOCH_2CH_2OH$, and CH_3OCH_2OH on electron exposure at 20 eV; Figure S12–S15, dependence of the formation of CH_4, CH_3CH_2OH, CH_3OCH_3, and CH_3OCH_2OH on electron exposure at 8 eV; Figure S16, ESD of H_2 upon electron exposure of CH_3OH at 13 eV.

Author Information

Corresponding Author

*E-mail: jhbredehoeft@uni-bremen.de

Notes

The authors declare no competing financial interest.

Acknowledgments

The work presented here was funded by the Deutsche Forschungsgemeinschaft DFG under project number SW26/15-2.

References

(1) Öberg, K. I. Photochemistry and Astrochemistry: Photochemical Pathways to Interstellar Complex Organic Molecules. *Chem. Rev.* **2016**, *116* (17), 9631–9663. https://doi.org/10.1021/acs.chemrev.5b00694.

(2) Boamah, M. D.; Sullivan, K. K.; Shulenberger, K. E.; Soe, C. M.; Jacob, L. M.; Yhee,

F. C.; Atkinson, K. E.; Boyer, M. C.; Haines, D. R.; Arumainayagam, C. R. Low-Energy Electron-Induced Chemistry of Condensed Methanol: Implications for the Interstellar Synthesis of Prebiotic Molecules. *Faraday Discuss.* **2014**, *168*, 249–266. https://doi.org/10.1039/c3fd00158j.

(3) Boyer, M. C.; Boamah, M. D.; Sullivan, K. K.; Arumainayagam, C. R.; Bazin, M.; Bass, A. D.; Sanche, L. Dynamics of Dissociative Electron-Molecule Interactions in Condensed Methanol. *J. Phys. Chem. C* **2014**, *118* (39), 22592–22600. https://doi.org/10.1021/jp506365d.

(4) Lepage, M.; Michaud, M.; Sanche, L. Low Energy Electron Total Scattering Cross Section for the Production of CO Within Condensed Methanol. *J. Chem. Phys.* **1997**, *107* (9), 3478–3484. https://doi.org/10.1063/1.474485.

(5) Jay-Gerin, J.-P.; Fraser, M.-J.; Swiderek, P.; Michaud, M.; Ferradini, C.; Sanche, L. Evidence for CO Formation in Irradiated Methanol and Acetone: Contribution of Low-Energy Electron-Energy-Loss Spectroscopy to γ-Radiolysis. *Radiat. Phys. Chem.* **1997**, *50* (3), 263–265.

(6) Sullivan, K. K.; Boamah, M. D.; Shulenberger, K. E.; Chapman, S.; Atkinson, K. E.; Boyer, M. C.; Arumainayagam, C. R. Low-Energy (<20 eV) and High-Energy (1000 eV) Electron-Induced Methanol Radiolysis of Astrochemical Interest. *Mon. Not. R. Astron. Soc.* **2016**, *460* (1), 664–672. https://doi.org/10.1093/mnras/stw593.

(7) Bennett, C. J.; Chen, S.; Sun, B.; Chang, A. H. H.; Kaiser, R. I. Mechanistical Studies on the Irradiation of Methanol in Extraterrestrial Ices. *Astrophys. J.* **2007**, *660* (2), 1588–1608. https://doi.org/10.1086/511296.

(8) Bennett, C. J.; Kaiser, R. I. On the Formation of Glycolaldehyde ($HCOCH_2OH$) and Methyl Formate ($HCOOCH_3$) in Interstellar Ice Analogs. *Astrophys. J.* **2007**, *661*, 899–909.

(9) Jheeta, S.; Domaracka, A.; Ptasinska, S.; Sivaraman, B.; Mason, N. J. The Irradiation of Pure CH_3OH and 1:1 Mixture of NH_3:CH_3OH Ices at 30 K Using Low Energy Electrons. *Chem. Phys. Lett.* **2013**, *556*, 359–364. https://doi.org/10.1016/j.cplett.2012.11.074.

(10) Maity, S.; Kaiser, R. I.; Jones, B. M. Infrared and Reflectron Time-of-Flight Mass Spectroscopic Study on the Synthesis of Glycolaldehyde in Methanol (CH_3OH) and Methanol-Carbon Monoxide (CH_3OH-CO) Ices Exposed to Ionization Radiation. *Faraday Discuss.* **2014**, *168*, 485–516. https://doi.org/10.1039/c3fd00121k.

(11) Maity, S.; Kaiser, R. I.; Jones, B. M. Formation of Complex Organic Molecules in Methanol and Methanol-Carbon Monoxide Ices Exposed to Ionizing Radiation – A Combined FTIR and Reflectron Time-of-Flight Mass Spectrometry Study. *Phys. Chem. Chem. Phys.* **2015**, *17* (5), 3081–3114. https://doi.org/10.1039/c4cp04149f.

(12) Zhu, C.; Turner, A. M.; Meinert, C.; Kaiser, R. I. On the Production of Polyols and

Hydroxycarboxylic Acids in Interstellar Analogous Ices of Methanol. *Astrophys. J.* **2020**, *889* (2), 134. https://doi.org/10.3847/1538-4357/ab6326.

(13) Harris, T. D.; Lee, D. H.; Blumberg, M. Q.; Arumainayagam, C. R. Electron-Induced Reactions in Methanol Ultrathin Films Studied by Temperature-Programmed Desorption: A Useful Method to Study Radiation Chemistry. *J. Phys. Chem.* **1995**, *99* (23), 9530–9535.

(14) Zhu, C.; Frigge, R.; Bergantini, A.; Fortenberry, R. C.; Kaiser, R. I. Untangling the Formation of Methoxymethanol (CH_3OCH_2OH) and Dimethyl Peroxide (CH_3OOCH_3) in Star-Forming Regions. *Astrophys. J.* **2019**, *881* (2), 156. https://doi.org/10.3847/1538-4357/ab2989.

(15) Chen, Y.-J.; Ciaravella, A.; Muñoz Caro, G. M.; Cecchi-Pestellini, C.; Jiménez-Escobar, A.; Juang, K.-J.; Yih, T.-S. Soft X-Ray Irradiation of Methanol Ice: Formation of Products as a Function of Photon Energy. *Astrophys. J.* **2013**, *778* (162), 1–11. https://doi.org/10.1088/0004-637X/778/2/162.

(16) Öberg, K. I.; Garrod, R. T.; van Dishoeck, E. F.; Linnartz, H. Formation Rates of Complex Organics in UV Irradiated CH_3OH-Rich Ices. *Astron. Astrophys.* **2009**, *504* (3), 891–913. https://doi.org/10.1051/0004-6361/200912559.

(17) Gerakines, P. A.; Schutte, W. A.; Ehrenfreund, P. Ultraviolet Processing of Interstellar Ice Analogs. *Astron. Astrophys.* **1996**, *312*, 289–305.

(18) Schneider, H.; Caldwell-Overdier, A.; Coppieters 't Wallant, S.; Dau, L.; Huang, J.; Nwolah, I.; Kasule, M.; Buffo, C.; Mullikin, E.; Widdup, L.; et al. Detection of Methoxymethanol as a Photochemistry Product of Condensed Methanol. *Mon. Not. R. Astron. Soc. Lett.* **2019**, *485* (1), L19–L23. https://doi.org/10.1093/mnrasl/slz019.

(19) Abou Mrad, N.; Duvernay, F.; Chiavassa, T.; Danger, G. Methanol Ice VUV Photoprocessing: GC-MS Analysis of Volatile Organic Compounds. *Mon. Not. R. Astron. Soc.* **2016**, *458* (2), 1234–1241. https://doi.org/10.1093/mnras/stw346.

(20) Baratta, G. A.; Castorina, A. C.; Leto, G.; Palumbo, M. E.; Spinella, F.; Strazzulla, G. Ion Irradiation Experiments Relevant to the Physics of Comets. *Planet. Space Sci.* **1994**, *42* (9), 759–766. https://doi.org/10.1016/0032-0633(94)90118-X.

(21) Hudson, R. L.; Moore, M. H. IR Spectra of Irradiated Cometary Ice Analogues Containing Methanol: A New Assignment, a Reassignment, and a Nonassignment. *Icarus* **2000**, *145* (2), 661–663. https://doi.org/10.1006/icar.2000.6377.

(22) Moore, M. H.; Ferrante, R. F.; Nuth, J. A. Infrared Spectra of Proton Irradiated Ices Containing Methanol. *Planet. Space Sci.* **1996**, *44* (9), 927–935. https://doi.org/10.1016/0032-0633(95)00120-4.

(23) De Barros, A. L. F.; Domaracka, A.; Andrade, D. P. P.; Boduch, P.; Rothard, H.; da Silveira, E. F. Radiolysis of Frozen Methanol by Heavy Cosmic Ray and Energetic Solar Particle Analogues. *Mon. Not. R. Astron. Soc.* **2011**, *418* (2), 1363–1374.

https://doi.org/10.1111/j.1365-2966.2011.19587.x.

(24) Modica, P.; Palumbo, M. E. Formation of Methyl Formate After Cosmic Ion Irradiation of Icy Grain Mantles. *Astron. Astrophys.* **2010**, *519*, A22. https://doi.org/10.1051/0004-6361/201014101.

(25) Abplanalp, M. J.; Förstel, M.; Kaiser, R. I. Exploiting Single Photon Vacuum Ultraviolet Photoionization to Unravel the Synthesis of Complex Organic Molecules in Interstellar Ices. *Chem. Phys. Lett.* **2016**, *644*, 79–98. https://doi.org/10.1016/j.cplett.2015.11.029.

(26) Paardekooper, D. M.; Bossa, J. B.; Linnartz, H. Laser Desorption Time-of-Flight Mass Spectrometry of Vacuum UV Photo-Processed Methanol Ice. *Astron. Astrophys.* **2016**, *592*, A67. https://doi.org/10.1051/0004-6361/201527937.

(27) Arumainayagam, C. R.; Lee, H. L.; Nelson, R. B.; Haines, D. R.; Gunawardane, R. P. Low-Energy Electron-Induced Reactions in Condensed Matter. *Surf. Sci. Rep.* **2010**, *65* (1), 1–44. https://doi.org/10.1016/j.surfrep.2009.09.001.

(28) Böhler, E.; Warneke, J.; Swiderek, P. Control of Chemical Reactions and Synthesis by Low-Energy Electrons. *Chem. Soc. Rev.* **2013**, *42* (24), 9219–9231. https://doi.org/10.1039/c3cs60180c.

(29) Cooks, R. G. Bond Formation upon Electron-Impact. *Org. Mass Spectrom.* **1969**, *2* (5), 481–519. https://doi.org/10.1002/oms.1210020505.

(30) Moore, J. H.; Swiderek, P.; Matejcik, S.; Allan, M. Principles and Applications. In *Nanofabrication Using Focused Ion and Electron Beams*; Russel, P., Moshkalev, S., Utke, I., Eds.; Oxford University Press: New York, 2012; pp 184–225.

(31) Bolina, A. S.; Wolff, A. J.; Brown, W. A. Reflection Absorption Infrared Spectroscopy and Temperature Programmed Desorption Investigations of the Interaction of Methanol with a Graphite Surface. *J. Chem. Phys.* **2005**, *122* (4), 044713. https://doi.org/10.1063/1.1839554.

(32) Bolina, A. S.; Wolff, A. J.; Brown, W. A. Reflection Absorption Infrared Spectroscopy and Temperature-Programmed Desorption Studies of the Adsorption and Desorption of Amorphous and Crystalline Water on a Graphite Surface. *J. Phys. Chem. B* **2005**, *109* (35), 16836–16845. https://doi.org/10.1021/jp0528111.

(33) Smith, R. S.; Huang, C.; Wong, E. K. L.; Kay, B. D. The Molecular Volcano: Abrupt CCl_4 Desorption Driven by the Crystallization of Amorphous Solid Water. *Phys. Rev. Lett.* **1997**, *79* (5), 909–912. https://doi.org/10.1103/PhysRevLett.79.909.

(34) Schmidt, F.; Swiderek, P.; Bredehöft, J. H. Electron-Induced Formation of Ethyl Methyl Ether in Condensed Mixtures of Methanol and Ethylene. *J. Phys. Chem. A* **2019**, *123* (1), 37–47. https://doi.org/10.1021/acs.jpca.8b10209.

(35) Schmidt, F.; Swiderek, P.; Bredehöft, J. H. Formation of Formic Acid, Formaldehyde, and Carbon Dioxide by Electron-Induced Chemistry in Ices of Water

and Carbon Monoxide. *ACS Earth Space Chem.* **2019**, *3* (9), 1974–1986. https://doi.org/10.1021/acsearthspacechem.9b00168.

(36) Bouilloud, M.; Fray, N.; Bénilan, Y.; Cottin, H.; Gazeau, M. C.; Jolly, A. Bibliographic Review and New Measurements of the Infrared Band Strengths of Pure Molecules at 25 K: H_2O, CO_2, CO, CH_4, NH_3, CH_3OH, HCOOH and H_2CO. *Mon. Not. R. Astron. Soc.* **2015**, *451* (2), 2145–2160. https://doi.org/10.1093/mnras/stv1021.

(37) *Python*, version 3.8.1; Python Software Foundation, **2019**.

(38) van der Walt, S.; Colbert, S. C.; Varoquaux, G. The NumPy Array: A Structure for Efficient Numerical Computation. *Comput. Sci. Eng.* **2011**, *13*, 22–30.

(39) Jones, E.; Oliphant, T.; Peterson, P.; et al. SciPy: Open Source Scientific Tools for Python, **2001**, www.scipy.org, (accesed August, 28th, 2020).

(40) Stein, S. E. Mass Spectra, In *NIST Chemistry WebBook*; Linstrom, P. J., Mallard, W.G., Eds.; NIST Standard Reference Database Number 69; National Institute of Standards and Technology: Gaithersburg, MD, http://webbook.nist.gov (accesed Juli 17th, 2020).

(41) Burean, E.; Ipolyi, I.; Hamann, T.; Swiderek, P. Thermal Desorption Spectrometry for Identification of Products Formed by Electron-Induced Reactions. *Int. J. Mass Spectrom.* **2008**, *277* (1–3), 215–219. https://doi.org/10.1016/j.ijms.2008.04.026.

(42) Kim, Y.-K.; Rudd, M. E. Binary-Encounter-Dipole Model for Electron-Impact

Ionization. *Phys. Rev. A. At., Mol., Opt. Phys.* **1994**, *50* (50), 3954–3967.

(43) Hwang, W.; Kim, Y.-K.; Rudd, M. E. New Model for Electron-Impact Ionization Cross Sections of Molecules. *J. Chem. Phys.* **1996**, *104* (8), 2956–2966.

(44) Schmidt, M. W.; Baldrige, K. K.; Boatz, J. A.; Elbert, S. T.; Gordon, M. S.; Jensen, J. H.; Koseki, S.; Matsunaga, N.; Nguyen, K. A.; Su, S. General Atomic and Molecular Electronic Structure System. *J. Comput. Chem.* **1993**, *14*, 1347–1363.

(45) Gordon, M. S.; Schmidt, M. W. Theory and Applications of Computational Chemistry: The First Forty Years. In *Theory and Applications of Computational Chemistry: The First Forty Years*; Dykstra, C. E., Frenking, G., Kim, K. S., Scuseria, G. E., Eds.; Elsevier: Amsterdam, The Netherlands, 2005; pp 1167–1185.

(46) Sharon, G. L.; Rhoda, D. L.; Sherif, A. K. Ion Energetics Data. In *NIST Chemistry WebBook*, NIST Standard Reference Database No. 69; Linstrom, P. J., Mallard, W. G., Eds.; National Institute of Standards and Technology: Gaithersburg, MD. http://webbook.nist.gov, (accessed Juli 17th, 2020).

(47) Johnson, R. A.; Stanley, A. E. GC/MS and FT-IR Spectra of Methoxymethanol. *Appl. Spectrosc.* **1991**, *45* (2), 218–222. https://doi.org/10.1366/0003702914337551.

(48) Janoschek, R.; Rossi, M. J. Thermochemical Properties of Free Radicals From G3MP2B3 Calculations. *Int. J. Chem. Kin.* **2002**, *34* (9), 550–560.

https://doi.org/10.1002/kin.10082.

(49) Kendall, R. A.; Dunning, T. H.; Harrison, R. J. Electron Affinities of the First-Row Atoms Revisited. Systematic Basis Sets and Wave Functions. *J. Chem. Phys.* **1992**, *96* (9), 6796–6806. https://doi.org/10.1063/1.462569.

(50) Pople, J. A.; Head-Gordon, M.; Raghavachari, K. Quadratic Configuration Interaction. A General Technique For Determining Electron Correlation Energies. *J. Chem. Phys.* **1987**, *87* (10), 5968–5975. https://doi.org/10.1063/1.453520.

(51) Head-Gordon, M.; Pople, J. A.; Frisch, M. J. MP2 Energy Evaluation by Direct Methods. *Chem. Phys. Lett.* **1988**, *153* (6), 503–506. https://doi.org/10.1016/0009-2614(88)85250-3.

(52) Neese, F.; Wennmohs, F.; Becker, U.; Riplinger, C. The ORCA Quantum Chemistry Program. *J. Chem. Phys.* **2020**, *224108*, 1–18. https://doi.org/10.1063/5.0004608.

(53) Neese, F. The ORCA Program System. *WIREs Comput. Mol. Sci.* **2012**, *2* (1), 73–78. https://doi.org/10.1002/wcms.81.

(54) Goesmann, F.; Rosenbauer, H.; Bredehöft, J. H.; Cabane, M.; Ehrenfreund, P.; Gautier, T.; Giri, C.; Krüger, H.; Le Roy, L.; MacDermott, A. J.; et al. Organic Compounds on Comet 67P/Churyumov-Gerasimenko Revealed by COSAC Mass Spectrometry. *Science* **2015**, *349* (6247), aab0689.

(55) Warneke, J.; Swiderek, P. Electron-Induced Decomposition of Condensed Acetone

Studied by Quantifying Desorption and Retention of Volatile Products. *J. Phys. Chem. C* **2015**, *119* (16), 8725–8735. https://doi.org/10.1021/acs.jpcc.5b01167.

(56) Yu, K. Y.; McMenamin, J. C.; Spicer, W. E. UPS Measurements of Molecular Energy Level of Condensed Gases. *Surf. Sci.* **1975**, *50* (1), 149–156. https://doi.org/10.1016/0039-6028(75)90179-X.

(57) Woodruff, D. P. Characterising Molecules and Molecular Interactions on Surfaces. *Modern Techniques of Surface Science*, 3rd ed.; Cambridge University Press: Cambridge, **2016**; pp. 383–467.

(58) Kühn, A.; Fenzlaff, H. P.; Illenberger, E. Formation and Dissociation of Negative Ion Resonances in Methanol and Allylalcohol. *J. Chem. Phys.* **1988**, *88* (12), 7453–7458. https://doi.org/10.1063/1.454309.

(59) Curtis, M. G.; Walker, I. C. Dissociative Electron Attachment in Water and Methanol (5-14 EV). *J. Chem. Soc., Faraday Trans.* **1992**, *88* (19), 2805–2810. https://doi.org/10.1039/FT9928802805.

(60) Ibănescu, B. C.; May, O.; Monney, A.; Allan, M. Electron-Induced Chemistry of Alcohols. *Phys. Chem. Chem. Phys.* **2007**, *9* (24), 3163–3173. https://doi.org/10.1039/b704656a.

(61) Michaud, M.; Fraser, M.-J.; Sanche, L. Low-Energy Electron-Energy-Loss Spectroscopy of Solid Methanol : Vibrational and Electronic Excitations. *J. Chim.*

Phys. **1994**, *91*, 1223–1227. https://doi.org/10.1051/jcp/1994911223.

(62) Kundu, S.; Davis, D.; Prabhudesai, V. S.; Krishnakumar, E. Low Energy Electron Induced Reactions in Condensed Methanol. *J. Phys. Conf. Ser.* **2015**, *635*, 062002. https://doi.org/10.1088/1742-6596/635/6/062002.

(63) Nixon, K. L.; Pires, W. A. D.; Neves, R. F. C.; Duque, H. V.; Jones, D. B.; Brunger, M. J.; Lopes, M. C. A. Electron Impact Ionisation and Fragmentation of Methanol and Ethanol. *Int. J. Mass Spectrom.* **2016**, *404*, 48–59. https://doi.org/10.1016/j.ijms.2016.05.006.

(64) Shukla, A. K.; Stace, A. J. Intermolecular Ion-Molecule Reactions in Clusters. The Reactions of Aliphatic Alcohols. *J. Phys. Chem.* **1988**, *92* (9), 2579–2583. https://doi.org/10.1021/j100320a036.

(65) Samy El-Shall, M.; Marks, C.; Wayne Sieck, L.; Meot-Ner, M. Reactions and Thermochemistry of Protonated Methanol Clusters Produced by Electron Impact Ionization. *J. Phys. Chem.* **1992**, *96* (5), 2045–2051. https://doi.org/10.1021/j100184a007.

(66) Varela, K.; Hargreaves, L. R.; Ralphs, K.; Khakoo, M. A.; Winstead, C.; McKoy, V.; Rescigno, T. N.; Orel, A. E. Excitation of the 4 Lowest Electronic Transitions in Methanol by Low-Energy Electrons. *J. Phys. B At. Mol. Opt. Phys.* **2015**, *48* (11), 115208. https://doi.org/10.1088/0953-4075/48/11/115208.

(67) Dech, J. M.; Kedzierski, W.; McConkey, J. W. Metastable Fragment Production in Electron-Methanol Collisions. *J. Phys. B At. Mol. Opt. Phys.* **2020**, *53* (15). https://doi.org/10.1088/1361-6455/ab94c7.

(68) Donohue, D. E.; Schiavone, J. A.; Freund, R. S. Molecular Dissociation by Electron Impact: High Rydberg Fragments from Methane, Ethylene, and Ethane. *J. Chem. Phys.* **1977**, *67* (2), 759–768. https://doi.org/10.1063/1.434838.

(69) Hama, T.; Yokoyama, M.; Yabushita, A.; Kawasaki, M.; Wickramasinghe, P.; Guo, W.; Loock, H.-P.; Ashfold, M. N. R.; Western, C. M. Translational and Internal Energy Distributions of Methyl and Hydroxyl Radicals Produced by 157 nm Photodissociation of Amorphous Solid Methanol. *J. Chem. Phys.* **2009**, *131*, 224512. https://doi.org/10.1063/1.3259877.

(70) Hama, T.; Yokoyama, M.; Yabushita, A.; Kawasaki, M. Translational and Internal States of Hydrogen Molecules Produced From the Ultraviolet Photodissociation of Amorphous Solid Methanol. *J. Chem. Phys.* **2009**, *130*, 164505. https://doi.org/10.1063/1.3100961.

(71) Chen, Z.; Eppink, A. T. J. B.; Jiang, B.; Groenenboom, G. C.; Yang, X.; Parker, D. H. Product Pair Correlation in CH_3OH Photodissociation at 157 nm: The OH + CH_3 Channel. *Phys. Chem. Chem. Phys.* **2011**, *13* (6), 2350–2355. https://doi.org/10.1039/c0cp01794a.

(72) Prabhudesai, V. S.; Nandi, D.; Kelkar, A. H.; Krishnakumar, E. Functional Group Dependent Dissociative Electron Attachment to Simple Organic Molecules. *J. Chem. Phys.* **2008**, *128* (15), 154309. https://doi.org/10.1063/1.2899330.

(73) Lee, J.; Grabowski, J. J. Reactions of the Atomic Oxygen Radical Anion and the Synthesis of Organic Reactive Intermediates. *Chem. Rev.* **1992**, *92* (7), 1611–1647. https://doi.org/10.1021/cr00015a007.

(74) Martinez, O.; Yang, Z.; Demarais, N. J.; Snow, T. P.; Bierbaum, V. M. Gas-Phase Reactions of Hydride Anion, H^-. *Astrophys. J.* **2010**, *720* (1), 173–177. https://doi.org/10.1088/0004-637X/720/1/173.

(75) Bredehöft, J. H.; Böhler, E.; Schmidt, F.; Borrmann, T.; Swiderek, P. Electron-Induced Synthesis of Formamide in Condensed Mixtures of Carbon Monoxide and Ammonia. *ACS Earth Space Chem.* **2017**, *1* (1), 50–59. https://doi.org/10.1021/acsearthspacechem.6b00011.

(76) Tedder, J. M. The Interaction of Free Radicals With Saturated Aliphatic Compounds. *Q. Rev. Chem. Soc.* **1960**, *14*, 336–356.

(77) Parenteau, L.; Jay-Gerin, J. P.; Sanche, L. Electron-Stimulated Desorption of H^- Ions via Dissociative Electron Attachment in Condensed Methanol. *J. Phys. Chem.* **1994**, *98* (40), 10277–10281. https://doi.org/10.1021/j100091a050.

(78) Bomse, D. S.; Dougal, S.; Woodin, R. L. Multiphoton Ionization Studies of IR

Multiphoton Dissociation: Direct C-H Bond Cleavage in Methanol. *J. Phys. Chem.* **1986**, *90* (12), 2640–2646. https://doi.org/10.1021/j100403a016.

For TOC Only

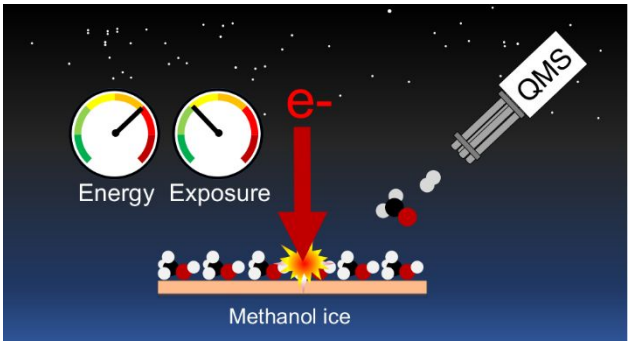

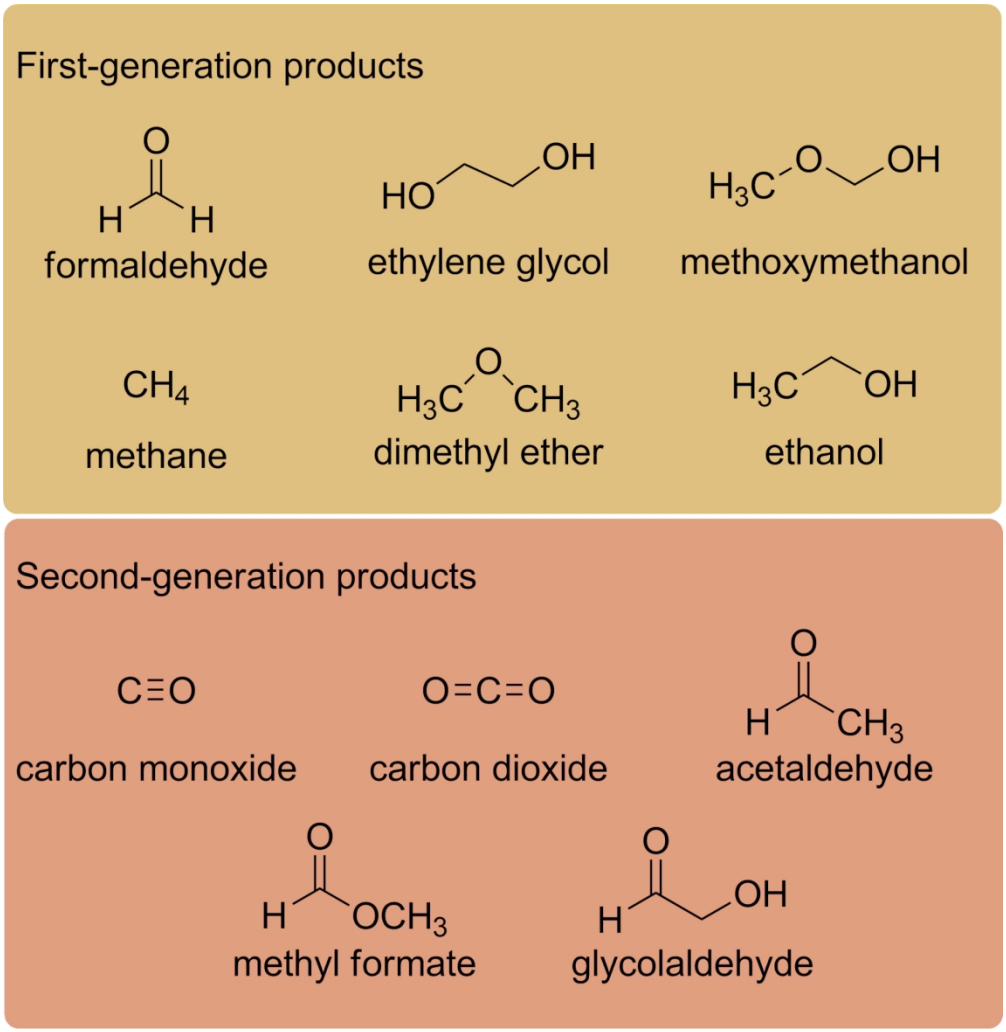

81x83mm (600 x 600 DPI)

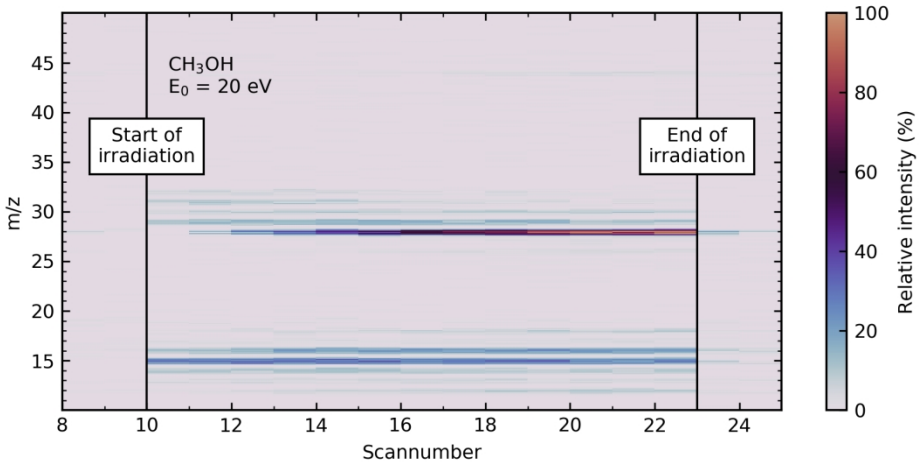

167x83mm (300 x 300 DPI)

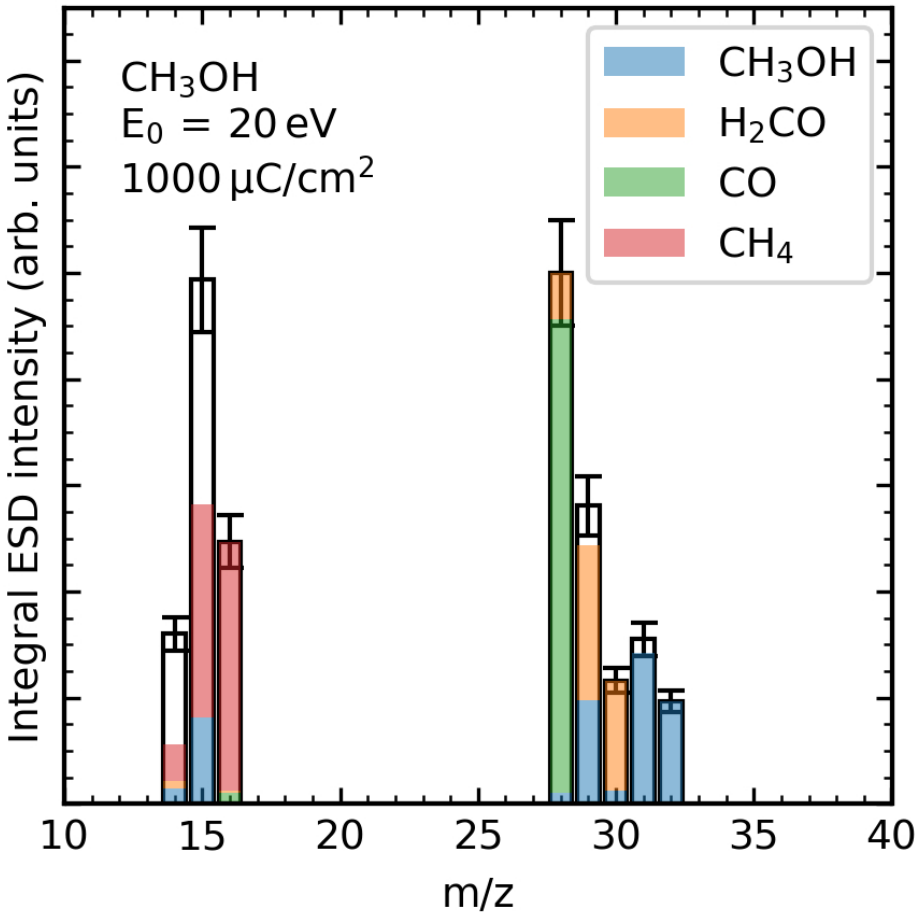

78x78mm (300 x 300 DPI)

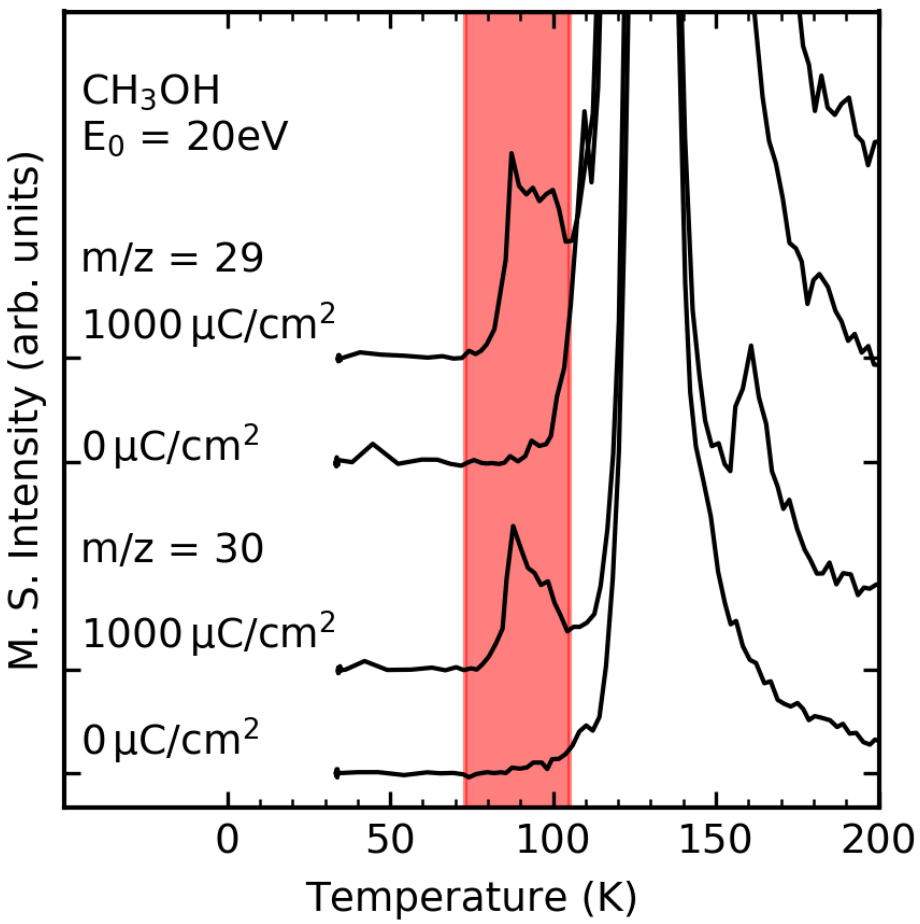

78x78mm (300 x 300 DPI)

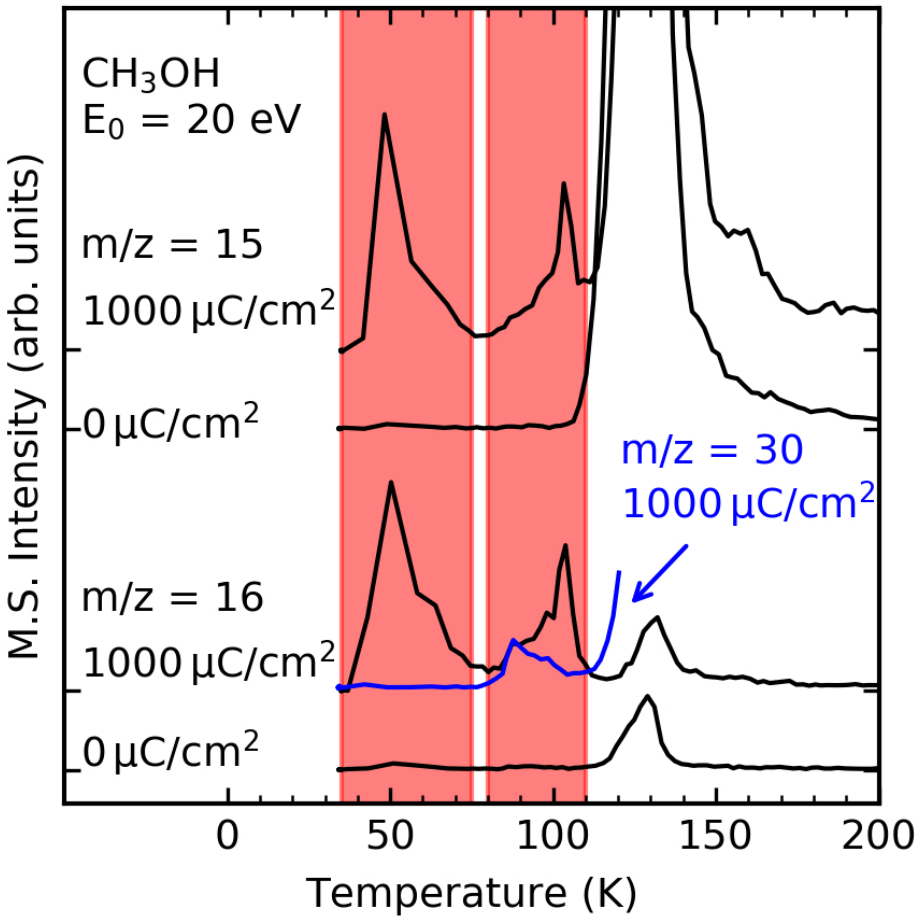

78x78mm (300 x 300 DPI)

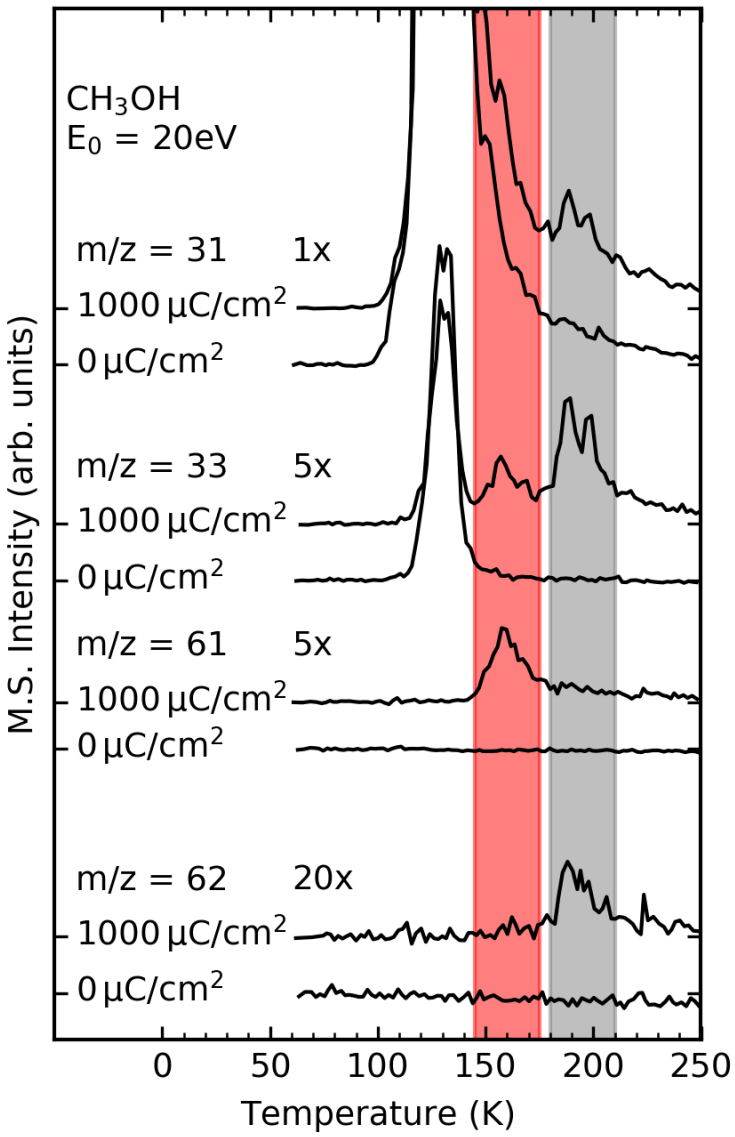

76x114mm (300 x 300 DPI)

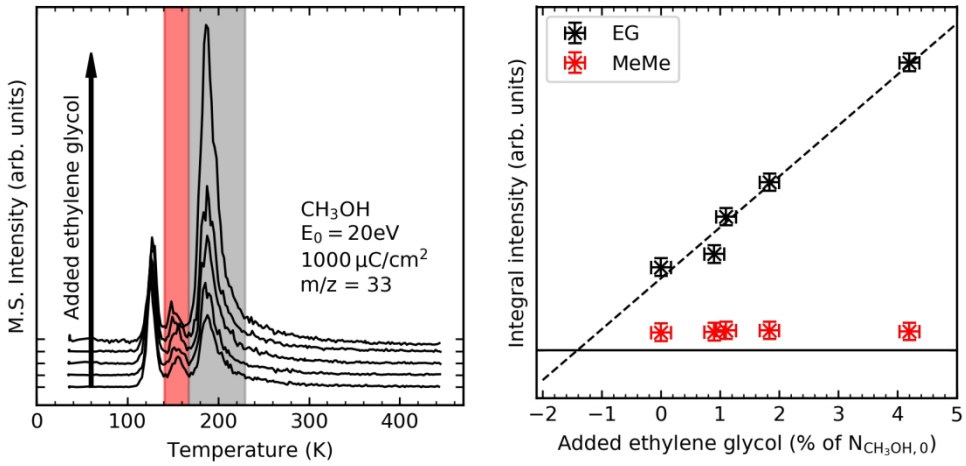

157x78mm (300 x 300 DPI)

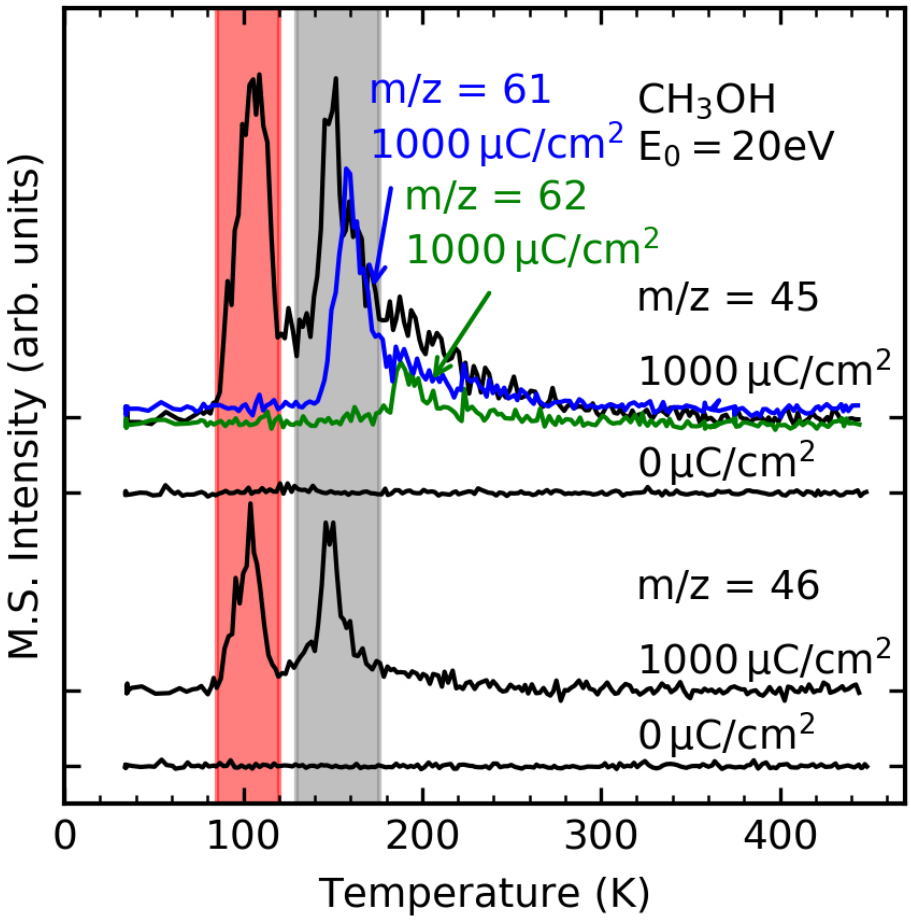

78x78mm (300 x 300 DPI)

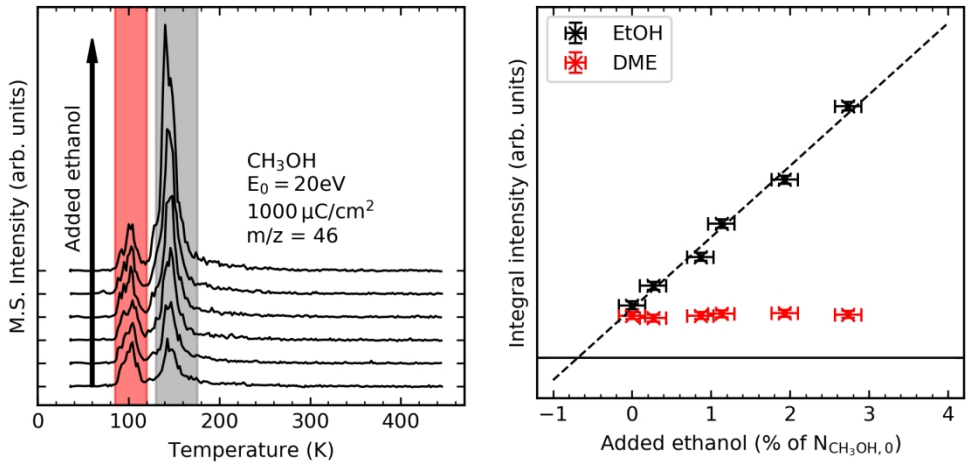

157x78mm (300 x 300 DPI)

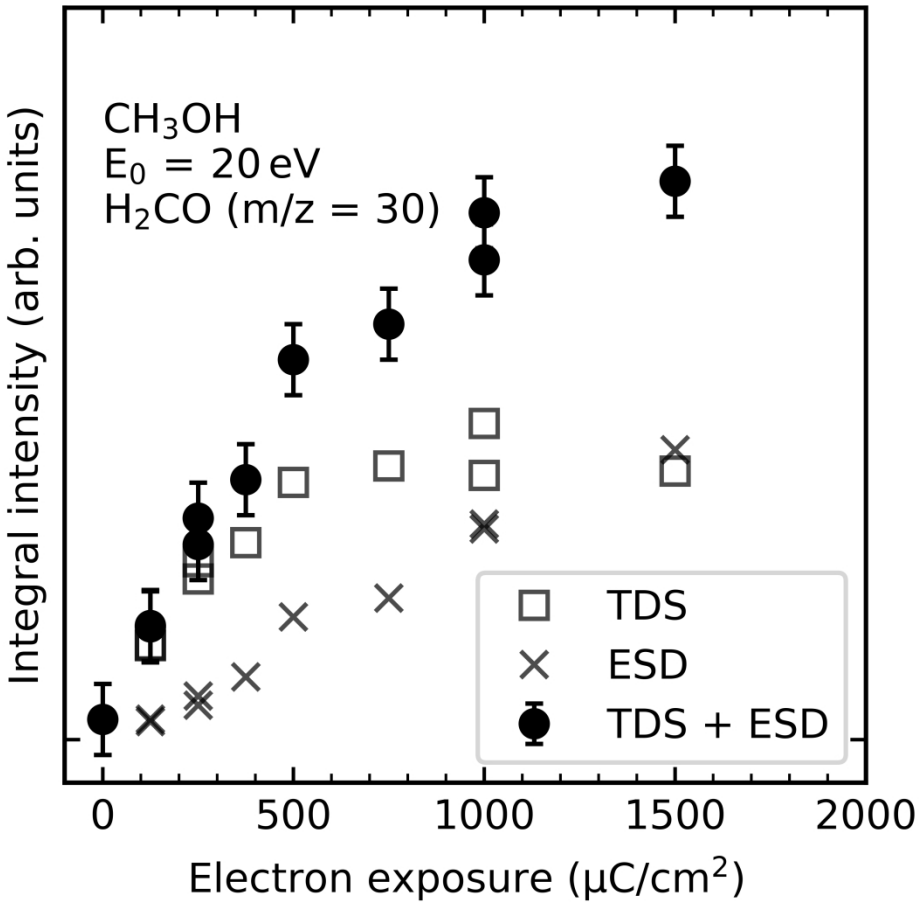

78x78mm (1200 x 1200 DPI)

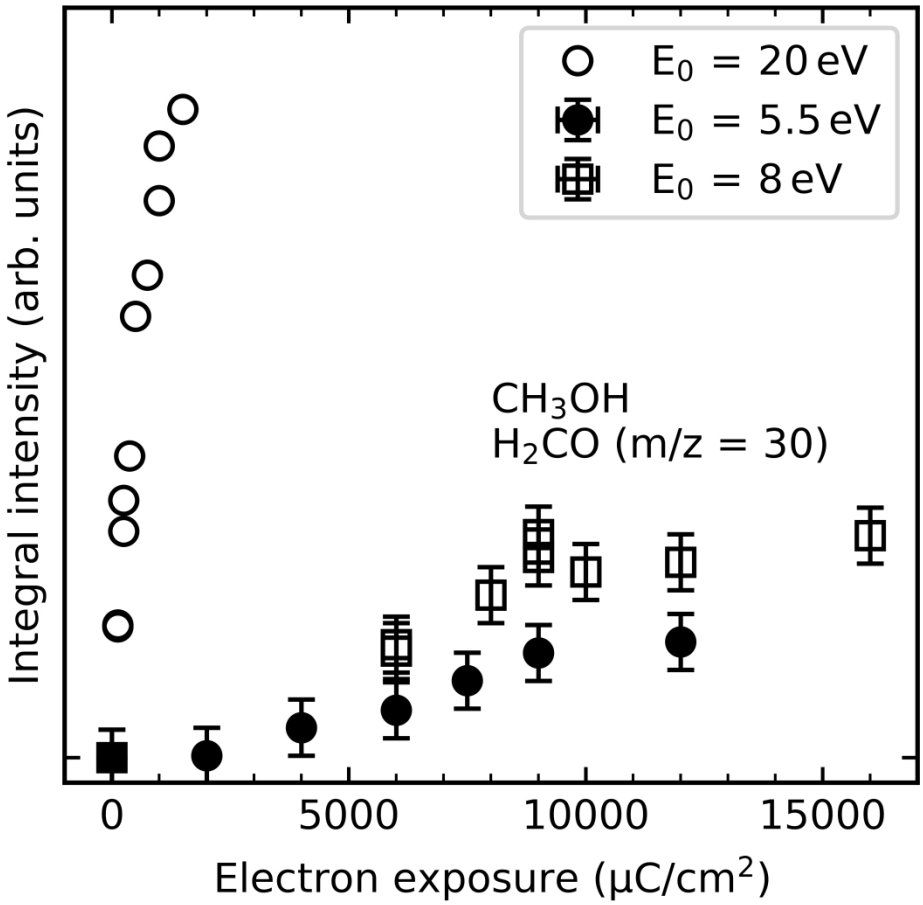

78x78mm (1200 x 1200 DPI)

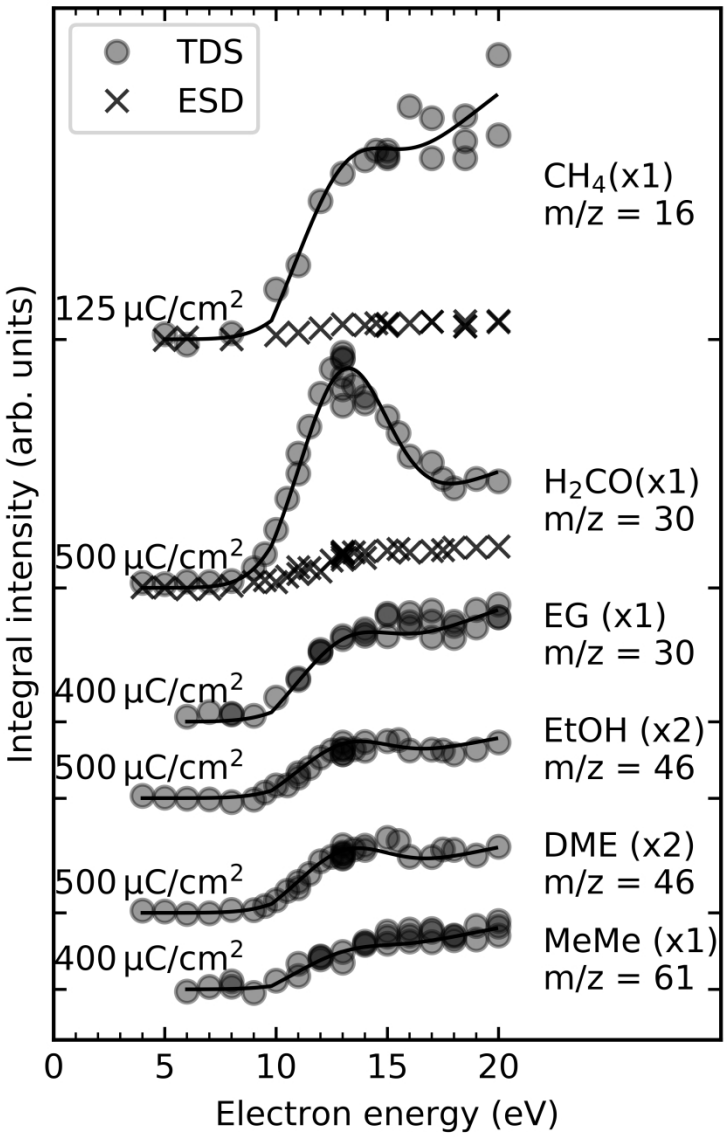

76x114mm (1200 x 1200 DPI)

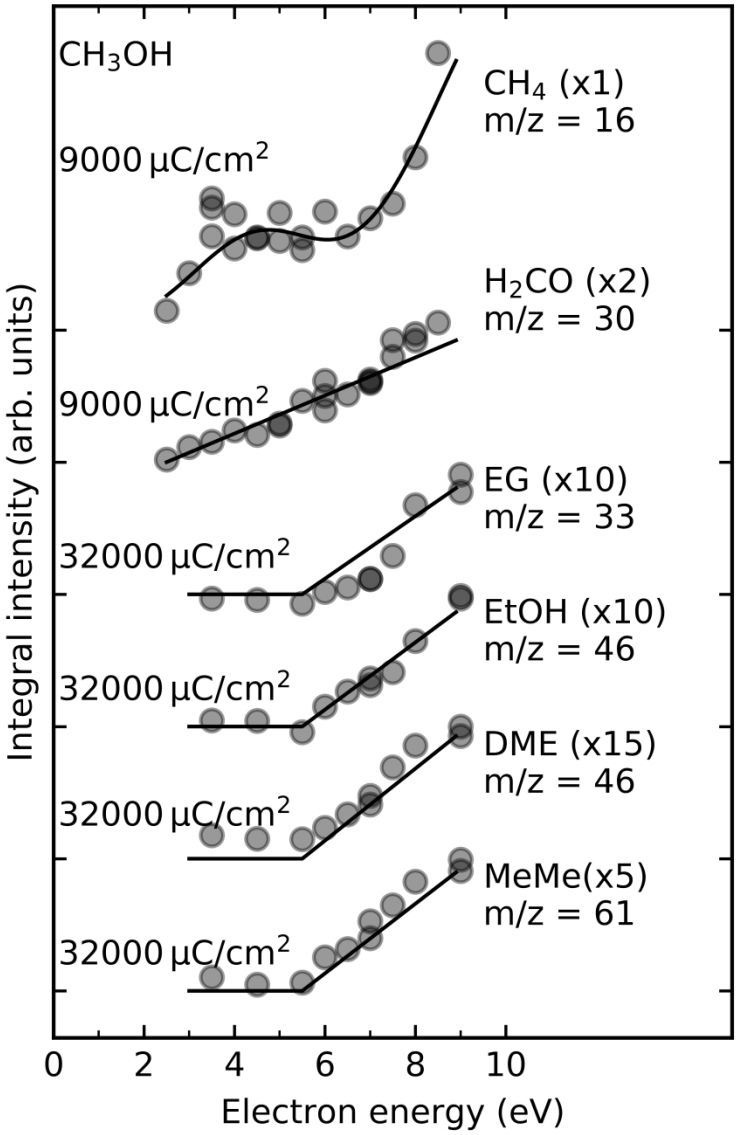

76x114mm (1200 x 1200 DPI)

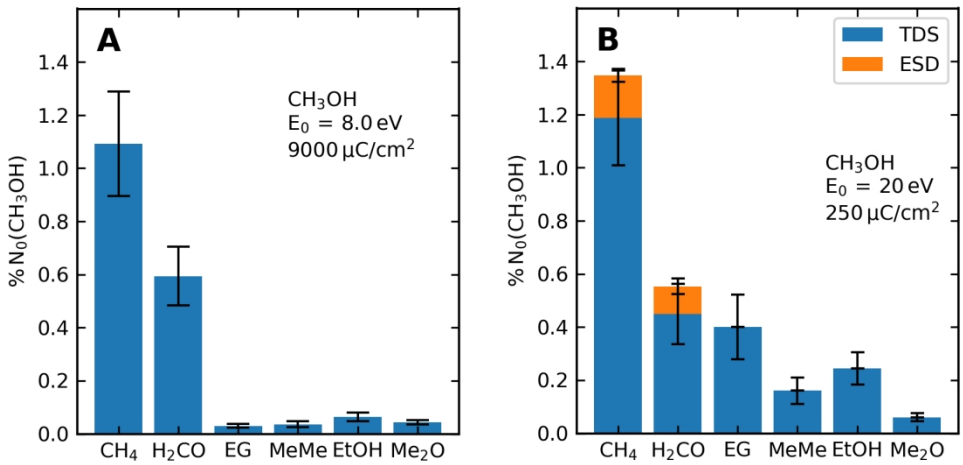

157x78mm (300 x 300 DPI)

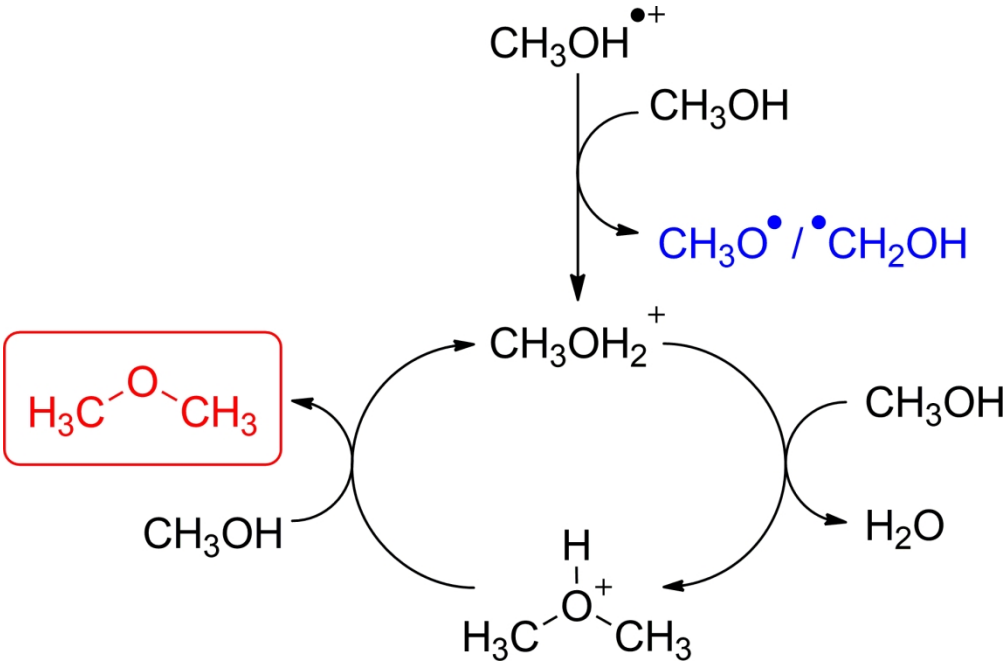

83x54mm (600 x 600 DPI)

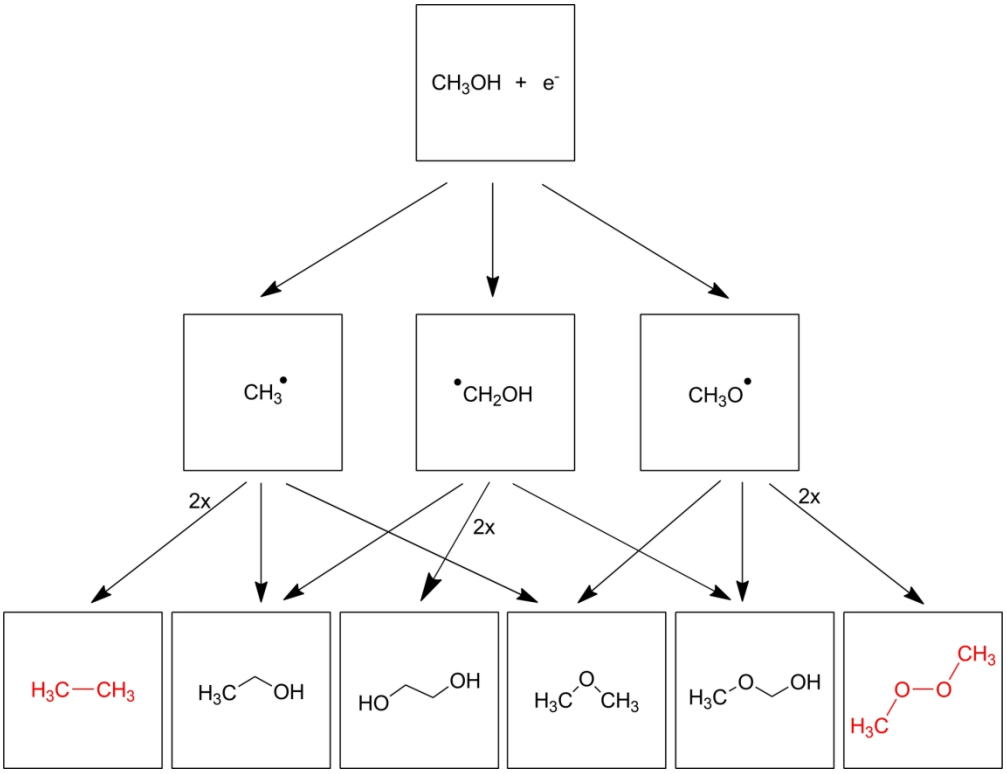

Scheme 2. Electron-molecule interactions lead to the formation of $CH_3^{\bullet}$, $^{\bullet}CH_2OH$, and $CH_3O^{\bullet}$ radicals which can recombine to yield $HOCH_2CH_2OH$, CH_3OCH_2OH, CH_3OCH_3, and CH_3CH_2OH. The potential recombination products ethane (C_2H_6) and dimethyl peroxide (CH_3OOCH_3) (red) have not been observed in the present study.

168x128mm (300 x 300 DPI)